Bovine herpesvirus 4-based vector delivering the full length xCT DNA efficiently protects mice from mammary cancer metastases by targeting cancer stem cells

Gaetano Donofrio[1], Giulia Tebaldi[1], Stefania Lanzardo[2], Roberto Ruiu[2], Elisabetta Bolli[2], Andrea Ballatore[2], Valeria Rolih[2], Francesca Macchi[1], Laura Conti[2*] & Federica Cavallo[2*]

[1]Department of Medical Veterinary Science, Università degli Studi di Parma, Parma, Italy. [1]Department of Molecular Biotechnology and Health Sciences, Molecular Biotechnology Center, Università degli Studi di Torino, Torino, Italy.

*These authors contributed equally.

Running title: Anti-xCT vaccination targets breast cancer stem cells

Keywords: Mammary Cancer, Cancer Stem Cell, xCT, Immunotherapy, Bovine herpesvirus 4-based vector

Financial Support: This work was supported by grants from the Italian Association for Cancer Research (IG 16724), Fondazione Ricerca Molinette Onlus, and by the Università degli Studi di Torino, Italy.

Corresponding authors:

Federica Cavallo

Università degli Studi di Torino, Department of Molecular Biotechnology and Health Sciences - Molecular Biotechnology Center, Via Nizza, 52 - 10126 - Torino, Italy

Phone: (+39) 011 6706457; Fax (+39) 011 236 6457;

e-mail: federica.cavallo@unito.it

and

Laura Conti

Università degli Studi di Torino, Department of Molecular Biotechnology and Health Sciences - Molecular Biotechnology Center, Via Nizza, 52 - 10126 – Torino, Italy

Phone: (+39) 011 6706458; Fax (+39) 011 670 6487;

e-mail: laura.conti@unito.it

Disclosure of interest: the authors declare that no potential conflicts of interest exist

Abstract

Despite marked advancements in its treatment, breast cancer is still the second leading cause of cancer death in women, due to relapses and distal metastases. Breast cancer stem cells (CSCs), are a cellular reservoir for recurrence, metastatic evolution and disease progression, making the development of novel therapeutics that target CSCs, and thereby inhibit metastases, an urgent need. We have previously demonstrated that the cystine-glutamate antiporter xCT (SLC7A11), a protein that was shown to be overexpressed in mammary CSCs and that plays a key role in the maintenance of their redox balance, self-renewal and resistance to chemotherapy, is a potential target for mammary cancer immunotherapy. This paper reports on the development of an anti-xCT viral vaccine that is based on the bovine herpesvirus 4 (BoHV-4) vector, which we have previously showed to be a safe vaccine that can transduce cells *in vivo* and confer immunogenicity to tumor antigens. We show that the vaccination of BALB/c mice with BoHV-4 expressing xCT (BoHV-4-mxCT), impaired lung metastases induced by syngeneic mammary CSCs both in preventive and therapeutic settings. Vaccination induced T lymphocyte activation and the production of anti-xCT antibodies that can mediate antibody-dependent cell cytotoxicity (ADCC), and directly impair CSC phenotype, self-renewal and redox balance. Our findings pave the way for the potential future use of BoHV-4 vectors that target xCT in metastatic breast cancer treatment.

Introduction

Breast cancer is a deadly disease that affects millions of women worldwide. Despite advances in diagnosis and treatment, it is still the second cause of cancer death in women worldwide [1]. Local and distant tumor recurrence occurs in a high percentage of patients and metastases are the main cause of mortality [2]. Novel therapies to treat metastatic breast cancer therefore become a necessity.

Recurrence and metastatic disease in breast cancer and most solid tumors have been ascribed to a small cancer cell population with stem-like properties, referred to as cancer stem cells (CSCs) [3]. CSCs escape cell cycle regulation and cell death, are endowed with unlimited self-renewal potential and tumor-initiating capacity as well as expressing epithelial to mesenchymal transition (EMT) markers, which enable them to migrate and initiate metastases. Moreover, CSCs overexpress many detoxifying enzymes and possess increased drug efflux and DNA repair capacities, which render them resistant to radiotherapy and cytotoxic drugs [4]. Much effort has therefore been dedicated to identifying novel targets and therapies to specifically impact CSCs [5].

We have identified the cystine-glutamate antiporter protein, xCT (SLC7A11), the light chain of the antiporter system x_c^-, as an oncoantigen (a tumor-associated antigen with a central role in cancer development and progression [6]), that is overexpressed in human and mouse mammary CSCs [7]. xCT plays an important role in maintaining intracellular redox balance, as it mediates the exchange of intracellular glutamate with extracellular cystine and thus promotes the synthesis of the anti-oxidant glutathione (GSH), thereby controlling intracellular reactive oxygen species (ROS), levels and chemosensitivity [8]. Moreover, xCT expression creates a reducing extracellular microenvironment, in a GSH-independent manner, by promoting a redox cycle in which cystine is taken up by cells and reduced to cysteine, some of which is secreted via constitutively expressed neutral amino acid transport systems [9]. Recent evidence shows that xCT also assists in protection from ferroptosis [8], and in cell metabolism regulation [10]. xCT is only expressed by a few normal cell types (astrocytes, microglia and some myeloid cells) [7], while it is overexpressed in numerous cancers, including a

high percentage of mammary tumors [11-15]. xCT expression has been observed in the CSCs of several cancer types, such as glioblastoma, colorectal, lung and gastric cancers [16], where it is stabilized on the cell membrane via interaction with two stem cell markers, Mucin-1 and CD44v [17]. xCT is therefore a promising target for the treatment of many cancers. In fact, research has demonstrated that xCT down-modulation and inhibition exert antitumor effects by impairing tumor growth and metastatic dissemination in preclinical models [18]. Moreover, preclinical experiments have shown that xCT disruption impairs the ROS defense system and sensitizes CSCs to chemotherapy, enhancing the therapeutic efficacy of doxorubicin, cisplatin and temozolomide [7, 19, 20]. This evidence has led to xCT inhibitors, either used in combination with chemotherapy or alone, being investigated in a number of clinical trials on cancer patients. The most commonly used xCT inhibitor is sulfasalazine (SASP), an anti-inflammatory drug approved by the FDA and EMA for the treatment of inflammatory bowel disease, ulcerative colitis and Crohn's disease. However, SASP is poorly bioavailable, induces many side effects and is not xCT specific, since it also inhibits NF-kB *in vivo* [21]. This may explain why clinical trials involving SASP administration have not produced the expected results.

Our search for new means to disrupt xCT functionality in CSCs has focused on active immunotherapy; anti-cancer vaccines are a promising strategy, as suggested by the advanced clinical testing that several have undergone in recent years[22, 23 24]. We have previously demonstrated that a DNA-based vaccine that expresses the full-length murine (m)xCT protein [7], and a virus-like particle, which displays the sixth extracellular loop of human xCT [25], induce an anti-xCT humoral response in BALB/c mice that was able to impair murine and human mammary CSC self-renewal *in vitro* and hinder mammary tumor growth and lung metastases in syngeneic tumor models. We herein explore Bovine Herpes Virus-4 (BoHV-4) use as a viral vector to deliver the full length xCT DNA, as we have previously demonstrated it is superior to DNA vaccination in inducing an anti-HER2 antibody response in tolerant HER2 transgenic BALB-neuT mice [26]. Moreover, BoHV-4

vaccination has the potential to induce an immune response against various xCT epitopes as our DNA vaccine, but does not require electroporation, avoiding the use of anesthetics and concerns about patients' compliance.

The immunization of mice with a BoHV-4 vector that expresses the full-length mxCT protein (BoHV-4-mxCT), induces T lymphocyte activation and the production of anti-xCT antibodies that can target CSCs both directly, by impairing self-renewal and increasing ROS content and ferroptosis, and via the induction of antibody-dependent cell cytotoxicity (ADCC). This immune response inhibited lung metastases that were either generated by the injection of CSCs derived from HER2/neu^{+} TUBO [27], or from triple negative 4T1 mammary cancer cells in syngeneic BALB/c mice, in preventive and therapeutic settings, respectively.

Results

Generation of a recombinant virus that delivers mxCT expression cassette

An optimized open reading frame (ORF), coding for mxCT (Slc7a11), was customized by adding a 33 aa peptide tag, derived from bovine herpesvirus-1 glycoprotein D (gD_{106}) [28] (Supplementary Fig. 1A), to its C-terminal to generate $mxCTgD_{106}$ ORF. $mxCTgD_{106}$ ORF was located downstream of the CMV promoter and upstream of the growth hormone polyadenylation signal to give the CMV-$mxCTgD_{106}$ expression cassette, whose functionality was tested via western blotting with a mAb to gD_{106}. CMV-$mxCTgD_{106}$ was excised from the plasmid backbone and sub-cloned into the pINT2 shuttle vector, which contained two BoHV-4 TK flanking sequences [29] (pTK-CMV-$mxCTgD_{106}$-TK), to generate pINT2-CMV-$mxCTgD_{106}$. This construct's protein expression was validated by transient transfection into HEK293T cells and immunoblotting (Supplementary Fig. 2). A genomic molecular clone, obtained from a BoHV-4 that was isolated from the milk cell fraction of a clinically healthy cow (designated as BoHV-4-A) [30], was used to generate the BoHV-4-A-CMV-$mxCTgD_{106}$ recombinant virus; pINT2-CMV-$mxCTgD_{106}$ was linearized and electroporated into SW102 *E. coli* cells that contained the artificial chromosome pBAC-BoHV-4-A-KanaGalKΔTK [30-

[36] (Fig. 1A), and heat-induced homologous recombination [37], generated pBAC-BoHV-4-A-CMV-mxCTgD$_{106}$. The TK locus of the BoHV-4 genome was chosen for its extreme stability after repeated *in vitro* and *in vivo* passages, and because it is reliable when integrating foreign DNA sequences into the BoHV-4 genome without any transgene or viral replication efficiency loss due to recombination. Viral particles were generated from pBAC-BoHV-4-A-CMV-mxCTgD$_{106}$, and the replication properties of BoHV-4-mxCT were compared to those of the parental BoHV-4-A virus. The replication rate of BoHV-4-mxCT is slightly lower than in BoHV-4-A (Fig. 1 D). However, BoHV-4-mxCT-transduced cells expressed mxCT, as revealed by western blotting (Fig. 1 E). A virus expressing the unrelated A29 Monkey poxvirus glycoprotein (BoHV-4-A29)[38] was used as a control.

BoHV-4-mxCT vaccination induces an anti-xCT humoral response

Sera from BoHV-4-mxCT- and BoHV-4-A29-vaccinated mice were collected, as was untreated mouse sera, 2 weeks after the last vaccination, and tested by ELISA. Figure 2A shows that BoHV-4-mxCT induced an antibody response against the mxCT protein. The sera were tested in ELISA for their ability to bind the extracellular portions of xCT to better evaluate the therapeutic potential of these antibodies. Fig. 2B-F demonstrates that BoHV-4-mxCT-induced antibodies recognized the extracellular domains of mouse xCT. Sera from BoHV-4-A29-vaccinated mice also bound, with a lower affinity, to full length mouse xCT and to its 6th extracellular loop (Fig. 2A, F), which could be explained by the identity of 3 residues in A29 and xCT 6th extracellular loop, which is sufficient to induce cross-reactivity [39]. BoHV-4-mxCT induced antibodies also recognized xCT protein in its native conformation, as shown by the decoration of xCT$^+$ tumorspheres by BoHV-4-mxCT-vaccinated mice sera (Fig. 2G). Finally, this binding ability resulted in the activation of ADCC against xCT$^+$ tumor cells, as demonstrated by incubating 4T1 target cells with the sera of BoHV-4-mxCT vaccinated mice in the presence of splenocytes from unvaccinated mice (Fig. 2H).

BoHV-4-mxCT-induced antibodies target CSCs and impair xCT function

To evaluate the direct effect exerted by BoHV-4-mxCT-induced antibodies on mammary CSCs, TUBO-derived tumorspheres were incubated for 5 days with sera from either control or vaccinated mice, or with the xCT inhibitor SASP (control). Whereas sera from untreated or BoHV-4-A29 vaccinated mice did not induce tumorsphere alterations, in terms of morphology, sphere number and dimension as compared with tumorspheres grown in medium alone, sera from mice vaccinated with BoHV-4-mxCT induced a reduction in sphere number and dimension. Tumorsphere dimension was further decreased by SASP treatment, suggesting that it is very efficient in slowing tumorsphere growth (Fig. 3A-C). BoHV-4-mxCT and SASP effects on tumorsphere generation were accompanied by a slight inhibition in cell cycle progression, as demonstrated by the increase in quiescent cells in the G0/G1 phase, when compared with control cells (Fig. 3D). BoHV-4-mxCT sera and SASP seemed to be able to target CSCs as they lowered the percentage of cells positive for the Aldefluor reagent, a non-immunological method to identify CSCs on the basis of their aldehyde dehydrogenase-1 (ALDH) activity (Fig. 3E, F). Indeed, high ALDH expression is considered a marker of CSC of various lineages, including breast cancer [40]. Moreover, both SASP and, to a greater extent, sera from BoHV-4-mxCT-treated mice altered CSC redox balance, inducing an intracellular ROS accumulation (Fig. 3G, H). The ROS content increase in cells treated with BoHV-4-mxCT-vaccinated mice sera or SASP was accompanied by an increase in ChaC glutathione-specific gamma-glutamylcyclotransferase 1 (Chac1) mRNA content (Fig. 3I), which is significantly elevated in cells undergoing endoplasmic reticulum stress and ferroptosis [8]. Interestingly, BoHV-4-mxCT-vaccinated mice sera and, to a greater extent, SASP, also upregulated xCT mRNA (Fig. 3L).

Overall, these results indicate that BoHV-4-mxCT vaccination induces the production of antibodies that alter CSC self-renewal and redox balance. These results were not confined to the TUBO model, since sera from BoHV-4-mxCT-vaccinated mice also reduced tumorsphere self-renewal, increased ROS content and decreased Aldefluor^{+} CSC number in 4T1 cells (Fig. 3M-O). Moreover, BoHV-4-mxCT-induced antibodies and, to a greater extent, SASP significantly inhibited glutamate export by

4T1 tumorspheres, reducing the amount of glutamate in the supernatant of treated tumorspheres to levels similar to those in epithelial 4T1 parental cells (Fig. 3P).

Interestingly, BoHV-4-mxCT-induced antibodies cross-reacted with human xCT, decreased CSC self-renewal and increased ROS content in human $HER2^{+}$ SKBR3 breast cancer cells (Supplementary Fig. 3).

Vaccination with BoHV-4-mxCT prevents TUBO lung metastases

To test the BoHV-4-mxCT-induced immune response's ability to prevent mammary CSC seeding in lungs, BALB/c mice were vaccinated twice, at two-week intervals, with BoHV-4-mxCT, or BoHV-4-A29 or left untreated (negative controls). After 7 days, mice were injected intravenously (i.v.), with syngeneic CSC-enriched [27], xCT^{+} TUBO tumorsphere-derived cells [7], and lung metastasis number was evaluated three weeks later. Whereas lungs from untreated and BoHV-4-A29-vaccinated mice showed a high number of macrometastases, lungs from BoHV-4-mxCT-vaccinated mice only displayed isolated macrometastases, as shown in Fig. 4A. These results were confirmed in a micrometastases analysis in H&E-stained lung sections (Fig. 4B), in which BoHV-4-mxCT-vaccinated mice showed a significant decrease in the percentage of lung tissue occupied by metastases (Fig. 4C), and in the number of metastases per square mm (Fig. 4D), relative to control mice. Overall, these data indicate that BoH-V-4-mediated xCT immunotargeting prevents mammary CSC seeding in the lungs.

Vaccination with BoHV-4-mxCT reduces mammary cancer growth and metastatic dissemination in a therapeutic setting

To investigate the ability of therapeutic vaccination to reduce tumor growth and spontaneous lung metastatization in mice with existing tumors, 4T1 tumorsphere-derived cells were transplanted subcutaneously (s.c.) into mice. When s.c. tumors reached 2 mm mean diameter, mice were vaccinated twice, at two week intervals. Tumor growth rate, measured as tumor volume progression over time, was significantly lower in the BoHV-4-mxCT vaccinated group than in the untreated and

198 BoHV-4-A29 vaccinated groups (Fig. 4E). Mice were culled, lungs harvested and subsequently
199 histologically analyzed twenty days after tumor cell challenge. BoHV-4-mxCT significantly
200 reduced the percentage of metastatic area and spontaneous micrometastasis number in the lungs
201 (Fig. 4F-H), suggesting that vaccination with BoHV-4-mxCT may be a new approach to mammary
202 cancer treatment.

203 **BoHV-4-mxCT induces T lymphocyte activation in the lungs of vaccinated mice.**

204 To further characterize the immune mechanisms that mediate BoHV-4-mxCT anti-metastatic
205 potential, the immune cell infiltrate in the lungs of vaccinated mice was analyzed three weeks after
206 TUBO-derived tumorsphere i.v. injection. $CD11b^+$ $Ly6G^+$ neutrophils and granulocytic myeloid-
207 derived suppressor cells (gMDSC) were the predominant myeloid cell population in metastatic
208 lungs, while $CD11b^+Ly6C^+$ monocytic myeloid-derived suppressor cells (mMDSC), $CD11b^+$
209 $F4/80^+$ macrophages and $CD11c^+$ dendritic cells only represented a minority. However, no
210 significant differences in myeloid cell population proportions were observed in the treatment groups
211 (Fig. 5A). The percentages of T lymphocytes ($CD3^+$), and Natural Killer (NK, $CD3^-CD49b^+$), cells
212 among the $CD45^+$ leucocytes did not vary significantly (Fig. 5B, G), and most T cells were $CD4^+$.
213 No significant $CD4^+/CD8^+$ T cell ratio alterations were detected, although both BoHV-4-A29 and
214 BoHV-4-mxCT slightly increased the $CD8^+$ cell percentage in the $CD3^+$ T cell population (Fig. 5C).
215 Interestingly, BoHV-4-mxCT vaccination induced T cell activation, as suggested by the significant
216 increase in $CD69^+$ cells in the total $CD3^+$ T cell population (Fig. 5D), and in both $CD4^+$ T helper ,
217 and $CD8^+$ T cytotoxic cells (Fig. 5D, H). Moreover, BoHV-4-mxCT significantly increased the
218 expression of immune checkpoint and exhaustion marker molecule PD1 in $CD4^+$, $CD8^+$ T and NK
219 cells (Fig. 5E, H). These data suggest that BoHV-4-mxCT vaccination may benefit from association
220 with anti-PD1 and/or anti-PDL1 monoclonal antibody therapy. In fact, PDL1 was expressed by a
221 small percentage of epithelial and myeloid cells in the lungs, and BoHV-4-A29 and BoHV-4-mxCT
222 vaccination slightly increased its expression in epithelial cells (Fig. 5F).

BoHV-4-mxCT vaccination induces the generation and expansion of effector T lymphocytes

To further characterize the T cell response induced by BoHV-4-mxCT vaccination, spleens from vaccinated mice that did not receive tumor cell injection were harvested and T cells were evaluated for their response against xCT. When splenocytes were re-stimulated with 15 μg/ml of H-2K^{d} dominant mouse xCT (S Y A E L G T S I) peptide [7], no specific IFN-γ production was detected by ELISPOT (data not shown), suggesting that high-avidity CD8^{+} T-cell clones could have been depleted during thymic selection, as we have previously reported for the Her2 antigen in the BALB-neuT model [41]. However, when splenocytes were cultured overnight with MitomycinC-treated xCT^{+} 4T1 cells, an increase in the percentage of CD4^{+} T cells expressing the CD69 activation marker was observed in BoHV-4-mxCT splenocytes (Fig. 6A), accompanied by a statistically significant increase in IFN-γ-producing helper T cells and a trend of increase in CD107^{+} cytotoxic CD4^{+} T cells (Fig. 6B, C). Activation and IFN-γ production were higher in CD8^{+} T cells from BoHV-4-mxCT vaccinated mice than in the untreated mice (Fig. 6D-F). The increased activation and IFN-γ production of both CD4^{+} and CD8^{+} T cells was maintained after 5 days of co-culture with 4T1 cells, when a statistically significant increase in CD107^{+} cytotoxic cells was also observed (Fig. 6G-N). To test the ability of these activated T cells to induce cytotoxicity in 4T1 cells, an *in vitro* killing assay was performed by co-culturing effector splenocytes from control, BoHV-4-mxCT and BoHV-4-A29 vaccinated mice with CFSE-labeled 4T1 target cells for 48 hours. BoHV-4-A29 and BoHV-4-mxCT splenocytes displayed enhanced lytic activity compared to untreated-mice splenocytes, but only a mild increase in BoHV-4-mxCT splenocyte cytotoxic activity over that of BoHV-4-A29 was observed (Fig. 6O).

To evaluate *in vivo* the role of this vaccine-induced T cell response, vaccinated and control mice were depleted of CD4^{+} and CD8^{+} T cells, starting at the time of TUBO tumorsphere i.v. injection (Fig. 7). While no significant differences in the percentage of metastatic area (Fig. 7A) and the number of lung metastases (Fig. 7B) were found in untreated and BoHV-4-A29 vaccinated mice

following depletion, a significant increase in both parameters was observed in CD8 depleted mice vaccinated with BoHV-4-mxCT (Fig. 7A, B). A significant increase in the percentage of metastatic area was also found in CD4 depleted BoHV-4-mxCT vaccinated mice as compared to not-depleted vaccinated mice (Fig. 7A). Since we have previously shown that CSC-enriched TUBO tumorspheres downregulated MHC class I expression [42], we hypothesized that BoHV-4-mxCT-induced antibodies could induce their differentiation and subsequent MHC class I expression. To confirm this hypothesis, TUBO tumorspheres were cultured for 5 days in the presence of sera from untreated, BoHV-4-A29 or BoHV-4-mxCT vaccinated mice or with IgG purified from the sera of BoHV-4-mxCT vaccinated mice. As shown in Fig. 7C, both purified IgG and sera from BoHV-4-mxCT vaccinated mice induced a significant increase in MHC class I expression, as compared to the control conditions. However, MHC class I upregulation induced by BoHV-4-mxCT sera was significantly higher than that induced by purified IgG, suggesting that the effect of anti-xCT IgG is amplified by the presence of vaccination-induced cytokines. Sera from BoHV-4-mxCT vaccinated mice induced also a mild increase in MHC class II and Fas expression (Fig. 7C). It is thus conceivable that $CD4^+$ and, to a greater extent, $CD8^+$ cytotoxic T cells contribute to the anti-metastatic effects of BoHV-4-mxCT vaccination.

Discussion

The recent clinical successes of checkpoint blocking antibodies and the discovery of cancer neoantigens have renewed interest in immunotherapy, which is entering a golden age. However, therapeutic cancer vaccines have not yet provided the expected clinical results, which would intensify the search for better tumor antigens and vaccine formulations. Moreover, the discovery that CSCs are the main source of tumor recurrence highlights how developing vaccines towards CSC-expressed antigens may treat metastatic cancer. We have previously shown that xCT is overexpressed in breast CSCs, where it plays a key role in the maintenance of self-renewal and redox balance [7], making it a potential CSC oncoantigen. In physiological conditions, xCT expression is confined to specialized areas in the brain, spleen and thymus [43], while its expression is enhanced on tumor cells in pancreatic, gastrointestinal, glioblastoma and colorectal cancers [7]. Indeed, xCT provides increased antioxidant capability allowing cancer cells to grow and resist to chemo- and radiotherapy [20]. Therefore, in several cancers, increased xCT expression is predictive for poor survival [11], making its immune-targeting of great clinical interest.

We have previously demonstrated that xCT immune-targeting, by means of VLPs or DNA vaccination, induced a specific humoral response that hampered breast cancer growth and metastasis in preclinical models of triple negative and $HER2^{+}$ breast cancers. However, these immunotherapies did not induce specific T cell activation, since xCT is a self-tolerated antigen and thymic depletion of high-avidity T-cell clones can occur [7, 25].

This work has focused on viral-vectors as a means to breaking tolerance and inducing a strong immune response, and has developed a BoHV-4-based vaccine that targets xCT. We have previously demonstrated that BoHV-4 can be used to express exogenous antigens in various cell types in several animal species without pathogenicity or oncogenicity [32, 44]. Moreover, when engineered to express HER2-derived antigens, it can protect HER2 transgenic BALB-neuT mice from autochthonous mammary cancer [26].

290 A mouse xCT-expressing BoHV-4 vector was thus generated to inhibit the seeding of $HER2^+$ CSCs
291 to the lungs in BALB/c mice, preventing the formation of pulmonary metastases. Of greater clinical
292 interest is BoHV-4-mxCT's ability to decrease the cancer growth, spontaneous metastatic spreading
293 and lung metastasis formation induced by TNBC CSCs in a therapeutic setting, suggesting that it
294 may benefit the 30% of TNBC patients who display xCT expression [11].

295 Cancer metastasis formation is a complex, multistage event involving continuous and finely tuned
296 interplay between the microenvironment and cancer cells, while immune cell composition in the
297 target organ is key in metastatic cell seeding [6, 45]. BoHV-4-mxCT vaccination induced activated T
298 lymphocyte recruitment in metastatic lungs, and increased the percentage of $CD4^+$ and $CD8^+$ T cells
299 that secreted IFN-γ in response to re-stimulation with xCT^+ tumor cells. This is noteworthy because
300 T lymphocyte infiltration is associated with good prognosis in breast cancer patients, while the
301 activation of IFN-γ-producing T helper 1 and $CD8^+$ T cells is important for anti-cancer response [46].
302 The re-stimulation of splenocytes from BoHV-4-mxCT vaccinated mice with 4T1 cells also
303 increased the percentage of $CD107^+$ T cells. Nevertheless, only a very slight increase in the ability
304 of splenocytes to kill 4T1 cells *in vitro* was detected when compared with splenocytes from BoHV-
305 4-A29 control mice. Since CSCs down regulate MHC class I expression as an immune evasion
306 mechanism [42], $CD8^+$ cytotoxic T lymphocytes are only expected to play a marginal role in the
307 immune surveillance of CSC metastatic spreading. This was confirmed by the absence of any effect
308 of CD8 depletion in untreated and BoHV-4-A29 vaccinated mice. A different situation is found
309 after BoHV-4-mxCT vaccination. Indeed, the induction of a T helper 1 response by BoHV-4-mxCT
310 was accompanied by a specific humoral response, including polyclonal antibodies that can
311 recognize xCT extracellular loops and bind CSC-enriched tumorspheres. These anti-xCT antibodies
312 exert therapeutic activity through different mechanisms, one of which is induction of CSC
313 differentiation and MHC class I expression, which makes them sensitive to $CD8^+$ T cell killing.
314 Indeed, depletion of $CD8^+$ T cells in BoHV-4-mxCT vaccinated mice resulted in an increased

315 development of lung metastases after an i.v. challenge of TUBO tumorspheres. The T helper 1
316 response potentiates this effect through the release of IFN-γ that induces MHC class I expression.
317 Moreover, this cytokine has been shown to induce MHC class II expression in cancer cells in
318 TNBC and other tumors with a T cell infiltrate [46]. Indeed, in our model the sera from BoHV-4-
319 mxCT vaccinated mice led to upregulation of MHC class II expression in TUBO tumorspheres, and
320 $CD4^+$ cells depletion during the effector phase of vaccine-induced immune response slightly
321 increased metastasis growth. This suggests the participation to immune response of $CD4^+$ cytotoxic
322 T lymphocytes, a cell population recently shown to lyse infected and neoplastic cancer cells in an
323 MHC class II dependent manner [47].

324 Vaccine-induced anti-xCT antibodies participate in tumor cell elimination by activating the innate
325 immune response via ADCC induction. Moreover, they can directly impair CSC self-renewal and
326 arrest their cell cycle in the G1 phase. BoHV-4-mxCT-induced antibodies alter CSC redox balance
327 by targeting xCT, which consequently increases intracellular ROS levels. Elevated ROS levels
328 hamper CSC survival by decreasing β-catenin activation and consequently down-regulating stem
329 cell genes, causing enhanced sensitivity to T cell cytotoxicity, as discussed above, chemo- and
330 radiotherapy, and ferroptosis; a recently discovered form of cell death caused by ROS and iron-
331 dependent lipid peroxide accumulation [48]. Indeed, elevated levels of the endoplasmic reticulum
332 stress and ferroptosis marker Chac1 [8], were observed in CSCs treated with sera from BoHV-4-
333 mxCT-vaccinated mice, confirming that this mechanism may contribute to BoHV-4-mxCT anti-
334 metastatic effect.

335 Moreover, as xCT mediates glutamate export in exchange with cystine, BoHV-4-mxCT-induced
336 antibodies lower extracellular glutamate levels. This makes the BoHV-4-mxCT vaccine an
337 interesting tool for the treatment of patients with bone metastasis, a common characteristic of
338 advanced breast cancer, since it has been demonstrated that glutamate released by cancer cells can
339 disrupt normal bone turnover, favoring metastasis formation and possibly causing cancer-induced

bone pain [49]. Moreover, high levels of extracellular glutamate have recently been shown to drive invasion through a paracrine signaling mediated by metabotropic glutamate receptors expressed in breast cancer cells [50].

Although xCT is a self-antigen, no overt adverse effects were observed in mice vaccinated with BoHV-4-mxCT, probably because its physiological expression is restricted to a few central nervous system and myeloid compartment cell types [7, 51]. The feasibility of xCT targeting in patients is supported by the extended usage of its inhibitor SASP in the clinical practice, for the treatment of many inflammatory diseases, without serious adverse events. Moreover, the safety of xCT immune targeting is further supported by the lack of immune infiltrate and abnormalities in the brains of mice vaccinated with VLPs that present xCT extracellular loops [25], and by the fact that xCT knockout mice display normal development and no organ alterations [52].

A comparison of the immune responses induced by BoHV-4-mxCT and by the DNA- and VLP-based vaccines we have previously used to target xCT requires additional experiments. However, from the data already available, it is clear that in all cases the main effector mechanism is represented by a T helper 1 immune response that results in anti-xCT IgG production [7, 25]. The highest specific antibody titer evaluated by ELISA was obtained with VLP vaccines, whose limitation - or advantage - is represented by the relatively small dimension of the xCT derived peptides they can display [53]. Instead, both DNA and BoHV-4 vaccines were designed to express the full length xCT protein, allowing the production of antibodies directed against different portions of xCT [53]. Moreover, while no specific T cell responses were detected in DNA and VLP vaccinated mice (even if no *in vivo* depletion experiments were performed) [7, 25], BoHV-4-mxCT induced a CD8 cytotoxic response, with a key role *in vivo*. This suggests that active immunization can be more effective than the passive administration of anti-xCT antibodies. Finally, despite inducing not completely identical immune responses, the anti-tumor and anti-metastatic efficacy of the three vaccines is very similar [7, 25]. This observation suggests that xCT immunotargeting, independently

on the vector used, slows tumor growth and decreases metastasis formation but is not able to completely eradicate the disease. Therefore, anti-xCT vaccination should be combined with other anti-cancer strategies. Indeed, it has become ever clearer that combination therapies provide better patient survival results than single agents. xCT immune-targeting may be used as an add-on therapy together with conventional and innovative treatments that can further stimulate immune responses targeting differentiated cancer cells/CSCs. Combinations with anti-PD1 or PD-L1 monoclonal antibodies may improve therapeutic efficacy as BoHV-4-mxCT enhances activation and consequently PD-1 expression on infiltrating T lymphocytes and we showed that PD-L1 is expressed on both CSCs and myeloid cells. The administration of anti-PD1 and anti-PD-L1 antibodies to breast cancer patients is currently undergoing clinical trial, and preliminary data show clinical activity in some TNBC patients treated with the anti-PD1 Pembrolizumab, (Keytruda; Merck; NCT01848834), and the anti-PD-L1 Atezolizumab (Tecentriq; Roche). Moreover, xCT targeting could be successfully coupled with chemotherapy, since many chemotherapeutic drugs eliminate differentiated cancer cells but expand CSCs by inducing a hypoxia-inducible factor (HIF)-1–dependent increase in xCT, leading to increased GSH and subsequent mitogen-activated protein kinase (MEK), inhibition and FoxO3 activation, which induces the transcription of Nanog and other stem-cell related genes [54]. In fact, we have previously demonstrated that combining anti-xCT DNA vaccination with doxorubicin significantly enhanced the anti-metastatic potential of the single treatments [7]. Since different signaling and metabolic pathways contribute to the maintenance of CSC phenotype and CSCs present a high degree of plasticity [4], another intriguing possibility would be a combination of multiple CSC-directed therapies to improve CSC elimination and prevent resistant clone onset. Using xCT immunotherapy together with metformin, a drug used to treat type 2 diabetes currently undergoing clinical trials in breast cancer patients, may exert a synergistic effect as xCT inhibition fosters the tricarboxylic acid (TCA) cycle by increasing intracellular glutamate levels, making cancer cells more resistant to glucose starvation [10]. This negative effect can be hindered by metformin's inhibition of the TCA cycle and mitochondrial respiration [55].

In conclusion, we have demonstrated that xCT immune-targeting via BoHV-4 based vectors is a safe strategy with which to target mammary CSCs and impair tumor growth and metastatic spread, making it a potential candidate for the further development of combination therapies that aim to prevent recurrence in breast cancer patients.

Materials and Methods:

Cell and tumorsphere cultures. 4T1 and SKBR3 cells were purchased from ATCC. TUBO cells were cultured as in [27]. Cells tested negative for mycoplasma [56], were passaged for fewer than 6 months. Tumorspheres were generated as in [27], and used at the second passage (P2), except where otherwise specified. Bovine embryo kidney cells (BEK), were provided by Dr. M. Ferrari, Istituto Zooprofilattico Sperimentale, Brescia, Italy; (BS CL-94). BEK cells that expressed cre recombinase (BEK*cre*), and HEK293T cells were cultured as in [32].

Generation of BoHV-4-mxCT. See Supplementary methods for details. Briefly, synthetic *Mouse xCT* ORF was amplified from SLC7a11 pDREAM 2.1 (GenScript), via PCR and cloned into the pIgKE2$_{BVD3}$gD$_{106}$ intermediate shuttle vector to generate CMV-mxCTgD$_{106}$ and then into pINT2-CMV-mxCTgD$_{106}$. EcoRI-linearized pINT2-CMV-mxCTgD$_{106}$ was used for heat-inducible homologous recombination in SW102 *E. coli* that contained the pBAC-BoHV-4-A-TK-KanaGalK-TK genome targeted to the TK locus with the KanaGalK selector cassette, as in [37]. Selected SW102 *E. coli* clones carrying pBAC-BoHV-4 recombinants were analyzed using HindIII restriction enzyme digestion and Southern blotting with a probe directed to the mxCT sequence [57]. BAC DNA (5 μg), was electroporated into BEK and BEK*cre* cells which were left to grow until the cytopathic effect (CPE), appeared. BoHV-4-mxCT and control BoHV-4-A29 were propagated by infecting BEK. Once CPE affected the majority of the cells, the virus was prepared by freezing and thawing cells three times before the virions were pelleted, using a 30% sucrose cushion [58], and then resuspended in EMEM.

FACS analysis

Tumorsphere-derived cells were stained using the Aldefluor kit (Stem Cell Technologies) [42], or with anti-H-2Kd-FITC, anti-Fas-PE/Cy7 (BD Bioscience), and anti-MHC class II-APC (Miltenyi Biotec) as in [42]. ROS content was measured using 2′,7′-dihydrochlorofluorescein diacetate (DHCF-DA, Sigma-Aldrich) [7]. Cells were incubated with 100µg/ml RNase A and 50µg/ml propidium iodide (Sigma-Aldrich) for 30 min for cell cycle analysis [59]. For immune infiltrate investigations, single cell suspensions were derived from vaccinated mice lungs [60], then stained with anti-CD45-VioGreen, anti-CD3-FITC, anti-CD4-APC-Vio770, anti-CD8-VioBlue, anti-CD49b-PE, anti-PD1-APC, anti-F4/80 -/Vio770, anti-CD11b-FITC, anti-Ly6G-Vioblue, anti-Ly6C-APC/Vio770 (Miltenyi Biotec), anti-CD69-PE/Vio770 (Biolegend), and anti-PDL1-PE (BD Bioscience), as in [61]. Samples were acquired on a BD FACSVerse and analyzed using BD FACSSuite software.

CD107 degranulation and IFN-γ production Assay

4T1 cells were incubated with 50µg/ml MitomycinC (Sigma-Aldrich), at 37°C for 2 hours, then washed 4 times and cultured overnight or for 5 days in RPMI10%FBS at $1x10^5$ cells/well with $1x10^6$ splenocytes recovered from untreated and vaccinated mice. In the last 4 hours, anti-CD107a/b-FITC Abs (BD Bioscience), and 10µg/ml brefeldinA (Sigma-Aldrich), were added. Cells were stained for surface antigens, fixed/permeabilized with the BD Cytofix/Cytoperm kit and stained with anti-IFN-γ-APC (BD Bioscience). Analyses were performed on $CD45^+$-gated lymphocytes with subsequent gating on either $CD4^+$ or $CD8^+$. Gates were set on T lymphocytes that had not been treated with brefeldinA and FMO samples [62].

Immunofluorescence

Tumorspheres were cytospinned to glass slides and stained with mouse sera (1:50), as in [7], and nuclei were stained with DAPI (Sigma-Aldrich). Images were acquired on a TCS-SP5II confocal

439 microscope and analyzed using LASAF software (Leica). Fluorescence was quantitated using
440 ImageJ and integrated density was normalized to nuclei number.

441 **ELISA**

442 Antibody responses were evaluated on plates coated with either mouse xCT protein (Cloud-Clone
443 Corp., 40 ng/well), human xCT protein (Abnova, 30 ng/well), or mouse xCT extracellular loop
444 peptides (GenScript, 1 µg/well). After blocking with 1%milk (Blotto, SantaCruz Biotechnology),
445 for 2 hours at 37°C, mouse sera (1:50), were incubated for 2 hours at 37°C. A standard curve was
446 generated for xCT proteins using a rabbit anti-xCT antibody (ThermoFisher). After 5 washes, HRP-
447 conjugated-anti-mouse and anti-rabbit IgG Abs (Sigma-Aldrich; 1:2,000), were incubated for 1
448 hour at 37°C. TMB (Sigma-Aldrich), was added after 5 washes. The reaction was stopped using 2N
449 HCl, and O.D. was measured at 450 nm using a 680XR microplate reader (BioRad).

450 **Glutamate quantification**

451 Glutamate was quantified in supernatants from 4T1 tumorspheres cultured for 5 days with mouse
452 sera (1:50), or SASP or from 4T1 cells using the Amplex Red glutamic acid/glutamate oxidase
453 assay kit (ThermoFisher), and was normalized to cell density.

454 **ADCC**

455 1×10^4 4T1 target cells were stained with 2 µM CFSE (Molecular Probes), cultured overnight with
456 untreated BALB/c mice splenocytes, used as effector cells (200:1, 100:1, and 50:1 E:T ratio), and
457 vaccinated mice sera (1:50). Cells were stained with 1µg/ml 7-AAD (BD Bioscience), and acquired
458 using FACS. %ADCC for each serum was calculated as in [25].

459 ***In vitro* cytotoxicity**

460 1×10^4 CFSE-labelled 4T1 target cells were incubated with splenocytes from untreated or vaccinated
461 mice as effector cells (200:1, 100:1, and 50:1 E:T ratio) for 48 hours, then harvested, stained with
462 1µg/ml 7-AAD, and acquired using FACS, as for ADCC.

463 **Immune sera effects on tumorsphere formation**

464 P1 tumorspheres were dissociated and either cultured with immunized mice sera (1:50), 50µM
465 SASP or nothing. After 5 days, P2 tumorspheres were imaged using a ApoTome fluorescence
466 microscope (Zeiss), and sphere diameter was measured using AxioVision 4.8 software [63]. Spheres
467 were counted, dissociated and processed for FACS analysis.

468 **RNA extraction and qPCR**

469 Total RNA was isolated from TUBO and 4T1 tumorspheres after 5 days of incubation with mouse
470 sera or SASP, and retrotranscribed to cDNA as in [27]. qPCR was performed with commercial
471 Slc7a11 and Gapdh (QuantiTect Primer Assay; Qiagen), or Chac1 custom primers [8], as in [27].
472 Slc7a11 and Chac1 expression levels were normalized on Gapdh, and expression levels were
473 calculated, relative to spheres incubated with untreated sera, using the comparative ΔΔCt method
474 and expressed as fold change.

475 ***In vivo* treatment**

476 Female 6-week-old BALB/c mice (Charles River Laboratories), were maintained at the Molecular
477 Biotechnology Center, University of Torino, in accordance with University Ethical Committee
478 guidelines and European Directive 2010/63. Vaccination, performed before (preventive model), or
479 after tumor challenge (therapeutic model), consisted of two i.p. injections of 10^6 TCID50 of either
480 BoHV-4-A29 or BoHV-4-mxCT at a 2-week interval. Two weeks after the second vaccination,
481 blood and spleens were collected from some mice, while others had $5x10^4$ TUBO-tumorsphere
482 derived cells injected i.v. and their lungs explanted 20 days later [7]. In the T cell depletion
483 experiment, mice were treated i.p. with PBS or 200 µg of anti-CD4 (clone GK1.5), anti-CD8 (clone
484 53-6.72) or isotype control antibodies (all from Bioxcell) every 3 days starting from cell challenge.
485 In the therapeutic model, $1x10^4$ 4T1 tumorsphere-derived cells were injected s.c. and the mice were
486 vaccinated when the tumor had reached 2 mm mean diameter. s.c. tumor growth was reported as
487 tumor volume. Mice were euthanized 20 days after cell challenge and lungs were removed [7]. Right

lungs were fixed in 4%formaldehyde, paraffin embedded, sectioned and H&E stained. Slides were digitized using a PannoramicDesk scanner and analyzed with PannoramicViewer1.15.4 (3D HISTECH). Two sections of each lung were prepared. In order to avoid double counting of the same lesion, the average of the values obtained by analyzing the two sections was calculated and then reported. Metastases and total lung area were determined using PannoramicViewer and ImageJ, respectively. The remaining lobes were processed for FACS.

Statistical analysis

Student's *t*-test was used. Data are shown as mean ± SEM unless otherwise stated. $P < 0.05$ was considered significant.

References

1. Siegel RL, Miller KD, Jemal A. Cancer Statistics, 2017. CA Cancer J Clin 2017; 67:7-30.
2. Colleoni M, Sun Z, Price KN, Karlsson P, Forbes JF, Thurlimann B, et al. Annual Hazard Rates of Recurrence for Breast Cancer During 24 Years of Follow-Up: Results From the International Breast Cancer Study Group Trials I to V. J Clin Oncol 2016; 34:927-35.
3. Peitzsch C, Tyutyunnykova A, Pantel K, Dubrovska A. Cancer stem cells: The root of tumor recurrence and metastases. Semin Cancer Biol 2017; 44:10-24.
4. Baccelli I, Trumpp A. The evolving concept of cancer and metastasis stem cells. J Cell Biol 2012; 198:281-93.
5. Lollini PL, Cavallo F, De Giovanni C, Nanni P. Preclinical vaccines against mammary carcinoma. Expert Rev Vaccines 2013; 12:1449-63.
6. Conti L, Ruiu R, Barutello G, Macagno M, Bandini S, Cavallo F, et al. Microenvironment, oncoantigens, and antitumor vaccination: lessons learned from BALB-neuT mice. Biomed Res Int 2014; 2014:534969.
7. Lanzardo S, Conti L, Rooke R, Ruiu R, Accart N, Bolli E, et al. Immunotargeting of Antigen xCT Attenuates Stem-like Cell Behavior and Metastatic Progression in Breast Cancer. Cancer Res 2016; 76:62-72.
8. de la Ballina LR, Cano-Crespo S, Gonzalez-Munoz E, Bial S, Estrach S, Cailleteau L, et al. Amino Acid Transport Associated to Cluster of Differentiation 98 Heavy Chain (CD98hc) Is at the Cross-road of Oxidative Stress and Amino Acid Availability. J Biol Chem 2016; 291:9700-11.
9. Conrad M, Sato H. The oxidative stress-inducible cystine/glutamate antiporter, system x (c) (-) : cystine supplier and beyond. Amino Acids 2012; 42:231-46.
10. Shin CS, Mishra P, Watrous JD, Carelli V, D'Aurelio M, Jain M, et al. The glutamate/cystine xCT antiporter antagonizes glutamine metabolism and reduces nutrient flexibility. Nat Commun 2017; 8:15074.
11. Timmerman LA, Holton T, Yuneva M, Louie RJ, Padro M, Daemen A, et al. Glutamine sensitivity analysis identifies the xCT antiporter as a common triple-negative breast tumor therapeutic target. Cancer Cell 2013; 24:450-65.
12. Lo M, Wang YZ, Gout PW. The x(c)- cystine/glutamate antiporter: a potential target for therapy of cancer and other diseases. J Cell Physiol 2008; 215:593-602.
13. Sugano K, Maeda K, Ohtani H, Nagahara H, Shibutani M, Hirakawa K. Expression of xCT as a predictor of disease recurrence in patients with colorectal cancer. Anticancer Res 2015; 35:677-82.

14. Cohen AS, Khalil FK, Welsh EA, Schabath MB, Enkemann SA, Davis A, et al. Cell-surface marker discovery for lung cancer. Oncotarget 2017; 8:113373-402.
15. Zhang L, Huang Y, Ling J, Zhuo W, Yu Z, Luo Y, et al. Overexpression of SLC7A11: a novel oncogene and an indicator of unfavorable prognosis for liver carcinoma. Future Oncol 2018.
16. Nagano O, Okazaki S, Saya H. Redox regulation in stem-like cancer cells by CD44 variant isoforms. Oncogene 2013; 32:5191-8.
17. Hasegawa M, Takahashi H, Rajabi H, Alam M, Suzuki Y, Yin L, et al. Functional interactions of the cystine/glutamate antiporter, CD44v and MUC1-C oncoprotein in triple-negative breast cancer cells. Oncotarget 2016; 7:11756-69.
18. Chen RS, Song YM, Zhou ZY, Tong T, Li Y, Fu M, et al. Disruption of xCT inhibits cancer cell metastasis via the caveolin-1/beta-catenin pathway. Oncogene 2009; 28:599-609.
19. Chen L, Li X, Liu L, Yu B, Xue Y, Liu Y. Erastin sensitizes glioblastoma cells to temozolomide by restraining xCT and cystathionine-gamma-lyase function. Oncol Rep 2015; 33:1465-74.
20. Ma MZ, Chen G, Wang P, Lu WH, Zhu CF, Song M, et al. Xc- inhibitor sulfasalazine sensitizes colorectal cancer to cisplatin by a GSH-dependent mechanism. Cancer Lett 2015; 368:88-96.
21. Weber CK, Liptay S, Wirth T, Adler G, Schmid RM. Suppression of NF-kappaB activity by sulfasalazine is mediated by direct inhibition of IkappaB kinases alpha and beta. Gastroenterology 2000; 119:1209-18.
22. Dillman RO. Is there a role for therapeutic cancer vaccines in the age of checkpoint inhibitors? Hum Vaccin Immunother 2017; 13:528-32.
23. Wong KK, Li WA, Mooney DJ, Dranoff G. Advances in Therapeutic Cancer Vaccines. Adv Immunol 2016; 130:191-249.
24. Lollini PL, De Giovanni C, Pannellini T, Cavallo F, Forni G, Nanni P. Cancer immunoprevention. Future Oncol 2005; 1:57-66.
25. Bolli E, O'Rourke JP, Conti L, Lanzardo S, Rolih V, Christen JM, et al. A Virus-Like-Particle immunotherapy targeting Epitope-Specific anti-xCT expressed on cancer stem cell inhibits the progression of metastatic cancer in vivo. OncoImmunology 2017:e1408746.
26. Jacca S, Rolih V, Quaglino E, Franceschi V, Tebaldi G, Bolli E, et al. Bovine herpesvirus 4-based vector delivering a hybrid rat/human HER-2 oncoantigen efficiently protects mice from autochthonous Her-2(+) mammary cancer. Oncoimmunology 2016; 5:e1082705.

562 27. Conti L, Lanzardo S, Arigoni M, Antonazzo R, Radaelli E, Cantarella D, et al. The
563 noninflammatory role of high mobility group box 1/Toll-like receptor 2 axis in the self-renewal of
564 mammary cancer stem cells. FASEB J 2013; 27:4731-44.
565 28. Capocefalo A, Franceschi V, Mertens PP, Castillo-Olivares J, Cavirani S, Di Lonardo E, et
566 al. Expression and secretion of Bluetongue virus serotype 8 (BTV-8)VP2 outer capsid protein by
567 mammalian cells. J Virol Methods 2010; 169:420-4.
568 29. Donofrio G, Cavirani S, Simone T, van Santen VL. Potential of bovine herpesvirus 4 as a
569 gene delivery vector. J Virol Methods 2002; 101:49-61.
570 30. Donofrio G, Sartori C, Franceschi V, Capocefalo A, Cavirani S, Taddei S, et al. Double
571 immunization strategy with a BoHV-4-vectorialized secreted chimeric peptide BVDV-E2/BoHV-1-
572 gD. Vaccine 2008; 26:6031-42.
573 31. Franceschi V, Capocefalo A, Cavirani S, Donofrio G. Bovine herpesvirus 4 glycoprotein B
574 is indispensable for lytic replication and irreplaceable by VSVg. BMC Vet Res 2013; 9:6.
575 32. Capocefalo A, Mangia C, Franceschi V, Jacca S, van Santen VL, Donofrio G. Efficient
576 heterologous antigen gene delivery and expression by a replication-attenuated BoHV-4-based
577 vaccine vector. Vaccine 2013; 31:3906-14.
578 33. Donofrio G, Sartori C, Ravanetti L, Cavirani S, Gillet L, Vanderplasschen A, et al.
579 Establishment of a bovine herpesvirus 4 based vector expressing a secreted form of the bovine viral
580 diarrhoea virus structural glycoprotein E2 for immunization purposes. BMC Biotechnol 2007; 7:68.
581 34. Franceschi V, Capocefalo A, Calvo-Pinilla E, Redaelli M, Mucignat-Caretta C, Mertens P,
582 et al. Immunization of knock-out alpha/beta interferon receptor mice against lethal bluetongue
583 infection with a BoHV-4-based vector expressing BTV-8 VP2 antigen. Vaccine 2011; 29:3074-82.
584 35. Redaelli M, Franceschi V, Capocefalo A, D'Avella D, Denaro L, Cavirani S, et al. Herpes
585 simplex virus type 1 thymidine kinase-armed bovine herpesvirus type 4-based vector displays
586 enhanced oncolytic properties in immunocompetent orthotopic syngenic mouse and rat glioma
587 models. Neuro Oncol 2012; 14:288-301.
588 36. Donofrio G, Franceschi V, Lovero A, Capocefalo A, Camero M, Losurdo M, et al. Clinical
589 protection of goats against CpHV-1 induced genital disease with a BoHV-4-based vector expressing
590 CpHV-1 gD. PLoS One 2013; 8:e52758.
591 37. Warming S, Costantino N, Court DL, Jenkins NA, Copeland NG. Simple and highly
592 efficient BAC recombineering using galK selection. Nucleic Acids Res 2005; 33:e36.
593 38. Franceschi V, Parker S, Jacca S, Crump RW, Doronin K, Hembrador E, et al. BoHV-4-
594 Based Vector Single Heterologous Antigen Delivery Protects STAT1(-/-) Mice from
595 Monkeypoxvirus Lethal Challenge. PLoS Negl Trop Dis 2015; 9:e0003850.

39. Craig L, Sanschagrin PC, Rozek A, Lackie S, Kuhn LA, Scott JK. The role of structure in antibody cross-reactivity between peptides and folded proteins. J Mol Biol 1998; 281:183-201.
40. Charafe-Jauffret E, Ginestier C, Iovino F, Tarpin C, Diebel M, Esterni B, et al. Aldehyde dehydrogenase 1-positive cancer stem cells mediate metastasis and poor clinical outcome in inflammatory breast cancer. Clin Cancer Res 2010; 16:45-55.
41. Rolla S, Nicolo C, Malinarich S, Orsini M, Forni G, Cavallo F, et al. Distinct and non-overlapping T cell receptor repertoires expanded by DNA vaccination in wild-type and HER-2 transgenic BALB/c mice. J Immunol 2006; 177:7626-33.
42. Tallerico R, Conti L, Lanzardo S, Sottile R, Garofalo C, Wagner AK, et al. NK cells control breast cancer and related cancer stem cell hematological spread. Oncoimmunology 2017; 6:e1284718.
43. Sato H, Tamba M, Ishii T, Bannai S. Cloning and expression of a plasma membrane cystine/glutamate exchange transporter composed of two distinct proteins. J Biol Chem 1999; 274:11455-8.
44. Verna AE, Franceschi V, Tebaldi G, Macchi F, Menozzi V, Pastori C, et al. Induction of Antihuman C-C Chemokine Receptor Type 5 Antibodies by a Bovine Herpesvirus Type-4 Based Vector. Front Immunol 2017; 8:1402.
45. Fusella F, Secli L, Busso E, Krepelova A, Moiso E, Rocca S, et al. The IKK/NF-kappaB signaling pathway requires Morgana to drive breast cancer metastasis. Nat Commun 2017; 8:1636.
46. Park IA, Hwang SH, Song IH, Heo SH, Kim YA, Bang WS, et al. Expression of the MHC class II in triple-negative breast cancer is associated with tumor-infiltrating lymphocytes and interferon signaling. PLoS One 2017; 12:e0182786.
47. Takeuchi A, Saito T. CD4 CTL, a Cytotoxic Subset of CD4(+) T Cells, Their Differentiation and Function. Front Immunol 2017; 8:194.
48. Ryoo IG, Lee SH, Kwak MK. Redox Modulating NRF2: A Potential Mediator of Cancer Stem Cell Resistance. Oxid Med Cell Longev 2016; 2016:2428153.
49. Fazzari J, Lin H, Murphy C, Ungard R, Singh G. Inhibitors of glutamate release from breast cancer cells; new targets for cancer-induced bone-pain. Sci Rep 2015; 5:8380.
50. Dornier E, Rabas N, Mitchell L, Novo D, Dhayade S, Marco S, et al. Glutaminolysis drives membrane trafficking to promote invasiveness of breast cancer cells. Nat Commun 2017; 8:2255.
51. Srivastava MK, Sinha P, Clements VK, Rodriguez P, Ostrand-Rosenberg S. Myeloid-derived suppressor cells inhibit T-cell activation by depleting cystine and cysteine. Cancer Res 2010; 70:68-77.

52. Sato H, Shiiya A, Kimata M, Maebara K, Tamba M, Sakakura Y, et al. Redox imbalance in cystine/glutamate transporter-deficient mice. J Biol Chem 2005; 280:37423-9.
53. Ruiu R, Rolih V, Bolli E, Barutello G, Riccardo F, Quaglino E, et al. Fighting breast cancer stem cells through the immune-targeting of the xCT cystine-glutamate antiporter. Cancer Immunol Immunother 2018, in press.
54. Lu H, Samanta D, Xiang L, Zhang H, Hu H, Chen I, et al. Chemotherapy triggers HIF-1-dependent glutathione synthesis and copper chelation that induces the breast cancer stem cell phenotype. Proc Natl Acad Sci U S A 2015; 112:E4600-9.
55. Hirsch HA, Iliopoulos D, Tsichlis PN, Struhl K. Metformin selectively targets cancer stem cells, and acts together with chemotherapy to block tumor growth and prolong remission. Cancer Res 2009; 69:7507-11.
56. Geninatti Crich S, Cadenazzi M, Lanzardo S, Conti L, Ruiu R, Alberti D, et al. Targeting ferritin receptors for the selective delivery of imaging and therapeutic agents to breast cancer cells. Nanoscale 2015; 7:6527-33.
57. Donofrio G, Franceschi V, Capocefalo A, Taddei S, Sartori C, Bonomini S, et al. Cellular targeting of engineered heterologous antigens is a determinant factor for bovine herpesvirus 4-based vaccine vector development. Clin Vaccine Immunol 2009; 16:1675-86.
58. Donofrio G, Cavaggioni A, Bondi M, Cavirani S, Flammini CF, Mucignat-Caretta C. Outcome of bovine herpesvirus 4 infection following direct viral injection in the lateral ventricle of the mouse brain. Microbes Infect 2006; 8:898-904.
59. Durelli L, Conti L, Clerico M, Boselli D, Contessa G, Ripellino P, et al. T-helper 17 cells expand in multiple sclerosis and are inhibited by interferon-beta. Ann Neurol 2009; 65:499-509.
60. Macagno M, Bandini S, Stramucci L, Quaglino E, Conti L, Balmas E, et al. Multiple roles of perforin in hampering ERBB-2 (Her-2/neu) carcinogenesis in transgenic male mice. J Immunol 2014; 192:5434-41.
61. Bandini S, Macagno M, Hysi A, Lanzardo S, Conti L, Bello A, et al. The non-inflammatory role of C1q during Her2/neu-driven mammary carcinogenesis. Oncoimmunology 2016; 5:e1253653.
62. Conti L, De Palma R, Rolla S, Boselli D, Rodolico G, Kaur S, et al. Th17 cells in multiple sclerosis express higher levels of JAK2, which increases their surface expression of IFN-gammaR2. J Immunol 2012; 188:1011-8.
63. Conti L, Lanzardo S, Ruiu R, Cadenazzi M, Cavallo F, Aime S, et al. L-Ferritin targets breast cancer stem cells and delivers therapeutic and imaging agents. Oncotarget 2016; 7:66713-27.

663 **Figure Legends**

664 **Figure 1. Generation of BoHV-4-mxCT. A)** Diagram (not to scale) showing the retargeting event
665 obtained by heat-inducible homologous recombination in SW102 *E. coli* containing pBAC-BoHV-
666 4-A-TK-KanaGalK-TK, where the Kana/GalK cassette was replaced with the CMV-mxCTgD_{106}
667 expression cassette flanked by BoHV-4 TK sequences, located in pINT2 shuttle plasmid vector. **B)**
668 Representative 2-deoxy-galactose resistant colonies tested by *HindIII* restriction enzyme analysis,
669 agar gel electrophoresis and Southern blotting performed with a specific probe for the mxCT ORF.
670 The 2,650 bp band (blue circle), corresponding to the un-retargeted pBAC-BoHV-4-A-TK-
671 KanaGalK-TK control, has been replaced by a 3156 bp band (red circle) in pBAC-BoHV-4-A-
672 CMV-mxCTgD_{106}ΔTK. **C)** Representative phase contrast and fluorescent microscopic images of
673 plaque formed by viable reconstituted recombinant BoHV-4-mxCT after the corresponding BAC
674 DNA electroporation into BEK cells expressing *cre* recombinase (Magnification, 10X). **D)**
675 Replication kinetics of BoHV-4-mxCT growth on BEK cells compared with the parental BoHV-4-
676 A isolate. The data presented are the means ± SEM of triplicate measurements ($P>0.05$ for all time
677 points as measured by Student's *t*-test). **E)** Western immunoblotting of cells infected with BoHV-4-
678 mxCT or the parental BoHV-4-A used as a negative control. The lanes were loaded with different
679 amounts of total protein cell extracts (5, 10 and 20 μl).

680 **Figure 2. BoHV-4-mxCT vaccination induces an anti-xCT humoral response.** Sera from
681 untreated (white bars), BoHV4-A29- (gray bars), and BoHV-4-mxCT- (black bars), vaccinated
682 mice were tested by ELISA on wells coated with **A)** full-length mouse xCT protein, or peptides
683 corresponding to mouse xCT extracellular loops **B)** 1, **C)** 2, **D)** 3, **E)** 4 or **F)** 6. Graphs show mean ±
684 SEM of sera pooled from 3 independent experiments. In A, antibody concentration was calculated
685 based on a standard curve obtained with a commercial anti-xCT antibody targeting its N-terminal
686 region. **G)** Representative immunofluorescence images of dissociated 4T1 tumorsphere cells
687 incubated with sera of vaccinated mice. The specific signal (green), was detected using an Alexa

Fluor488-conjugated anti-mouse secondary antibody. Nuclei were counterstained with DAPI (blue). Magnification 40X, Scale bar, 40 μm. **, $P < 0.01$, Student's *t*-test. **H)** ADCC assay performed using $CFSE^+$ 4T1 target cells incubated with 1:50 pooled sera from untreated, BoHV4-A29- and BoHV-4-mxCT-vaccinated mice and splenocytes from untreated mice as effector cells at different effector/target cells ratios (200:1, 100:1, and 50:1). Results shown are the mean ± SEM of the percentage of ADCC, calculated as in Material and Methods.

Figure 3. BoHV-4-mxCT induces antibodies to target CSC and affects self-renewal and ROS flux. TUBO **A-L)**- and 4T1 **M-P)**-derived tumorspheres were incubated for 5 days with medium, sera of BALB/c untreated BoHV-4-A29- and BoHV-4-mxCT-vaccinated mice, or with SASP (50 μM). **A)** Representative images of tumorspheres, magnification 40X, scale bar 40 μm. **B)** Sphere generating ability reported as tumorsphere number/10^3 plated cells. **C)** Sphere diameter measured with the AxioVision 4.8 software. **D)** Percentage of cells in the different phases of the cell cycle, as measured by FACS analysis using propidium iodide **E-F)** Aldefluor positivity reported as percentage of positive cells or as representative density plots. **G-H)** FACS analysis of ROS production, reported as DCF MFI or shown as representative histograms. **I-L)** Real time PCR of the ferroptosis marker Chac1 or of xCT. All graphs show mean ± SEM from at least three independent experiments. **M)** Sphere generating ability reported as tumorsphere number/10^3 plated cells. **N)** FACS analysis of ROS production, reported as DCF MFI. **O)** Aldefluor positivity reported as percentage of positive cells. **P)** Evaluation of glutamate in the supernatants of treated 4T1 tumorspheres or of parental 4T1 cells cultured as monolayers. *, $P < 0.05$; **, $P < 0.01$, ***, $P < 0.001$, Student's *t*-test.

Figure 4. Vaccination with BoHV-4-mxCT decreases mammary cancer lung metastases. A-D) BALB/c mice were vaccinated twice with BoHV-4-mxCT, BoHV-4-A29 or left untreated. One week after the final administration, TUBO-derived tumorspheres were injected into the tail vein of treated mice. 20 days after cell challenge, lungs were removed, sectioned and micrometastasis

number was determined in at least 2 H&E sections per mouse. **A)** Photograph of representative lungs, **B)** Representative images of lung metastases after H&E staining. Graphs showing **C)** the % of metastatic area and **D)** metastases number per square mm (sq mm), measured in mouse lungs from 3 independent experiments. **E-H**) BALB/c mice were s.c. challenged with 1 x 10^4 4T1 tumorsphere-derived cells. When the tumors reached 4 mm diameter, mice were vaccinated and boosted 14 days later. **E)** Subcutaneous tumor diameters were measured at the indicated time points and tumor volume was calculated. Graphs showing **F)** the % of metastatic area and **G)** the number of metastases per square mm measured in lungs. **H)** Representative images of lung metastases after H&E staining. *P<0.05, **P<0.01, Student's *t*-test.

Figure 5. BoHV-4-mxCT induces lung T lymphocyte activation in vaccinated mice. Cytofluorimetric analysis of lung immune infiltrates in untreated (white bars), BoHV4-A29- (gray bars) and BoHV-4-mxCT- (black bars), vaccinated mice**. A)** Graph shows the percentage ± SEM of $CD45^+$ myeloid cells expressing the markers of mMDSC ($CD11b^+Ly6C^+$), neutrophil/gMDSC ($CD11b^+Ly6G^+$), macrophage ($CD11b^+F4/80^+$), and dendritic cell ($CD11b^-CD11c^+$), populations. **B)** Graph shows the percentage ± SEM of $CD45^+$ cells expressing the markers of T ($CD3^+CD49b^-$), and NK ($CD3^-CD49b^+$), populations. **C)** Percentage ± SEM of $CD4^+$ or $CD8^+$ cells among the $CD45^+CD3^+$ T cell population. **D)** Percentage ± SEM of $CD69^+$ cells among total T, $CD4^+$ or $CD8^+$ T, and NK cell populations. **E)** Percentage ± SEM of $PD1^+$ cells among total T, $CD4^+$ or $CD8^+$ T, and NK cell populations. **F)** Percentage ± SEM of $PDL1^+$ cells among epithelial ($CD45^-$) or myeloid ($CD11b^+$) cells. **G-H)** Representative density plots showing **G)** CD3 and CD49b expression on $CD45^+$ cells, and **H)** CD69 and PD1 expression on $CD4^+$ or $CD8^+$ T lymphocytes . *, P < 0.05; **, P < 0.01, ***, P < 0.001, Student's *t*-test.

Figure 6. BoHV-4-mxCT vaccination induces degranulation and IFN-γ production in T lymphocytes. A-N) Splenocytes from untreated (white bars), BoHV4-A29- (gray bars), and BoHV-4-mxCT- (black bars), vaccinated mice, were co-cultured with mitomycin C treated 4T1 cells

overnight (**A-F**) or for 5 days (**G-N**), incubated with antibodies against CD107a and b FITC in the presence of Brefeldin A for 4 hours, then stained with antibodies against CD45, CD4, CD8, and CD69 and for intracellular IFN-γ and analyzed by FACS. Graphs show means ± SEM of the percentages of **A-C, G-I)** $CD4^+$ or **D-F, L-N)** $CD8^+$ cells expressing **A, D, G, L)** CD69, **B, E, H, M)** IFN-γ or **C, F, I, N)** CD107 from three experiments. **O)** Splenocytes from untreated, BoHV4-A29 and BoHV-4-mxCT vaccinated mice were co-cultured with $CFSE^+$ 4T1 cells for 48 hours, then the percentage of 7-AAD^+ dead cells among the $CFSE^+$ target populations was analyzed by FACS. Graphs shows mean ± SEM of the percentages of specific lysis, calculated as described in Material and Methods. *, $P < 0.05$; **, $P < 0.01$, ***, $P < 0.001$, Student's *t*-test.

Figure 7. Depletion of T lymphocytes impairs BoHV-4-mxCT anti-metastatic activity. A, B) BALB/c mice were vaccinated twice with BoHV-4-mxCT, BoHV-4-A29 or left untreated. One week after the final vaccination, TUBO-derived tumorspheres were injected intravenously. Mice were then treated i.p., every 3 days, with either PBS or 200 μg of anti-CD4, anti-CD8 or isotype control antibodies. 20 days after cell challenge, lungs were removed, sectioned and micrometastasis number was determined in H&E sections. Graphs showing means ± SEM of **A)** the % of metastatic area and **B)** metastasis number per square mm (sq mm) (n=5 per group). **C)** TUBO-derived tumorspheres were incubated for 5 days with medium, sera of untreated, BoHV-4-A29- or BoHV-4-mxCT-vaccinated BALB/c mice, or with IgG purified from sera from BoHV-4-mxCT-vaccinated mice (50 μg/ml). FACS analysis of MHC class I, MHC class II and Fas, reported as means ± SEM of MFI from three experiments. *, $P < 0.05$; **, $P < 0.01$, ***, $P < 0.001$, Student's *t*-test.

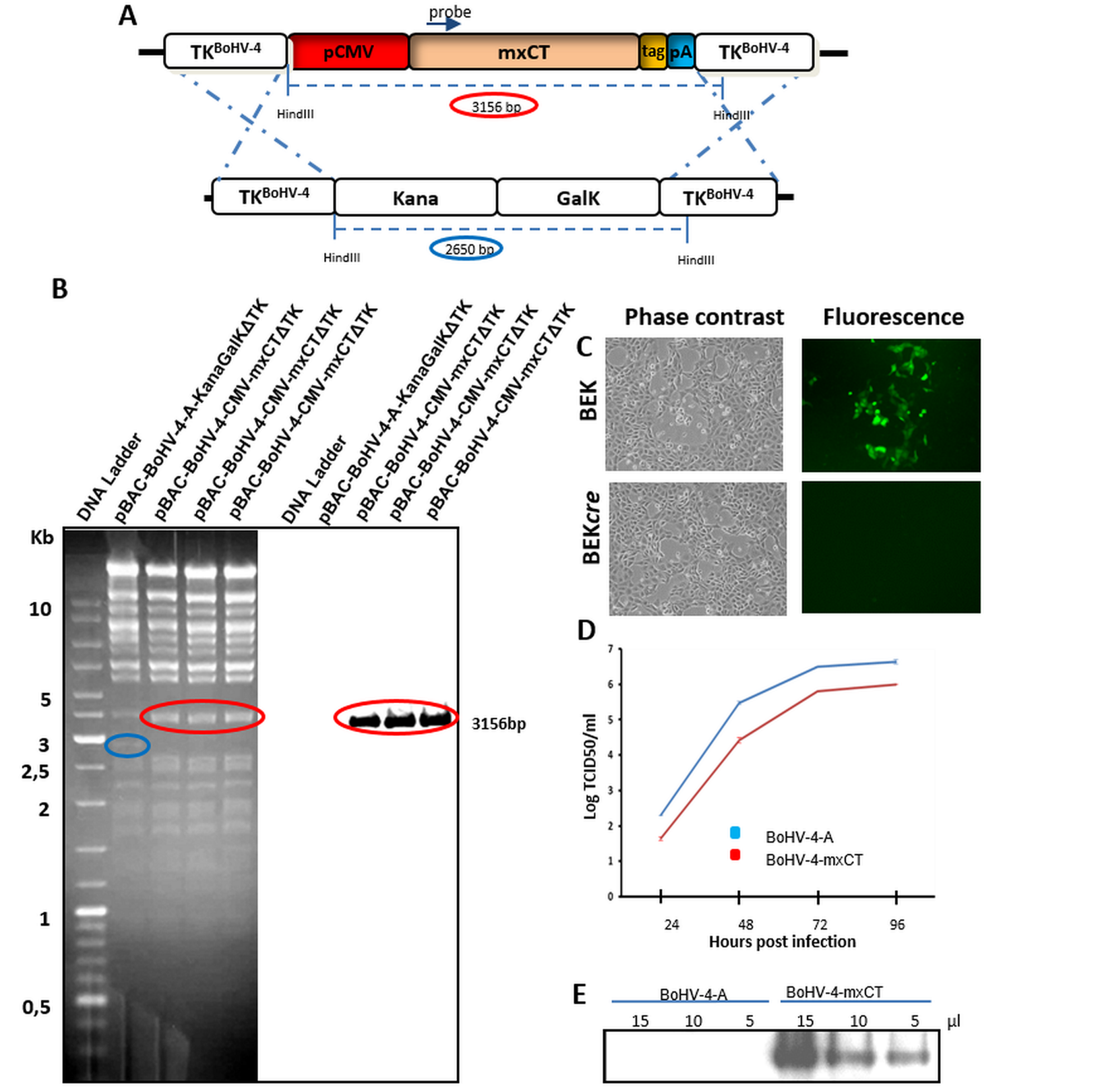
A
probe
TK BoHV-4
pCMV
mxCT
tag
pA
TK BoHV-4
HindIII
3156 bp
HindIII
TK BoHV-4
Kana
GalK
TK BoHV-4
HindIII
2650 bp
HindIII
B
DNA Ladder
pBAC-BoHV-4-A-KanaGalKΔTK
pBAC-BoHV-4-CMV-mxCTΔTK
pBAC-BoHV-4-CMV-mxCTΔTK
pBAC-BoHV-4-CMV-mxCTΔTK
pBAC-BoHV-4-CMV-mxCTΔTK
DNA Ladder
pBAC-BoHV-4-A-KanaGalKΔTK
pBAC-BoHV-4-CMV-mxCTΔTK
pBAC-BoHV-4-CMV-mxCTΔTK
pBAC-BoHV-4-CMV-mxCTΔTK
pBAC-BoHV-4-CMV-mxCTΔTK
Kb
10
5
3
2,5
2
1
0,5
3156bp
C
Phase contrast
Fluorescence
BEK
BEKcre
D
Log TCID50/ml
0
1
2
3
4
5
6
7
24
48
72
96
Hours post infection
BoHV-4-A
BoHV-4-mxCT
E
BoHV-4-A
BoHV-4-mxCT
15
10
5
15
10
5
µl

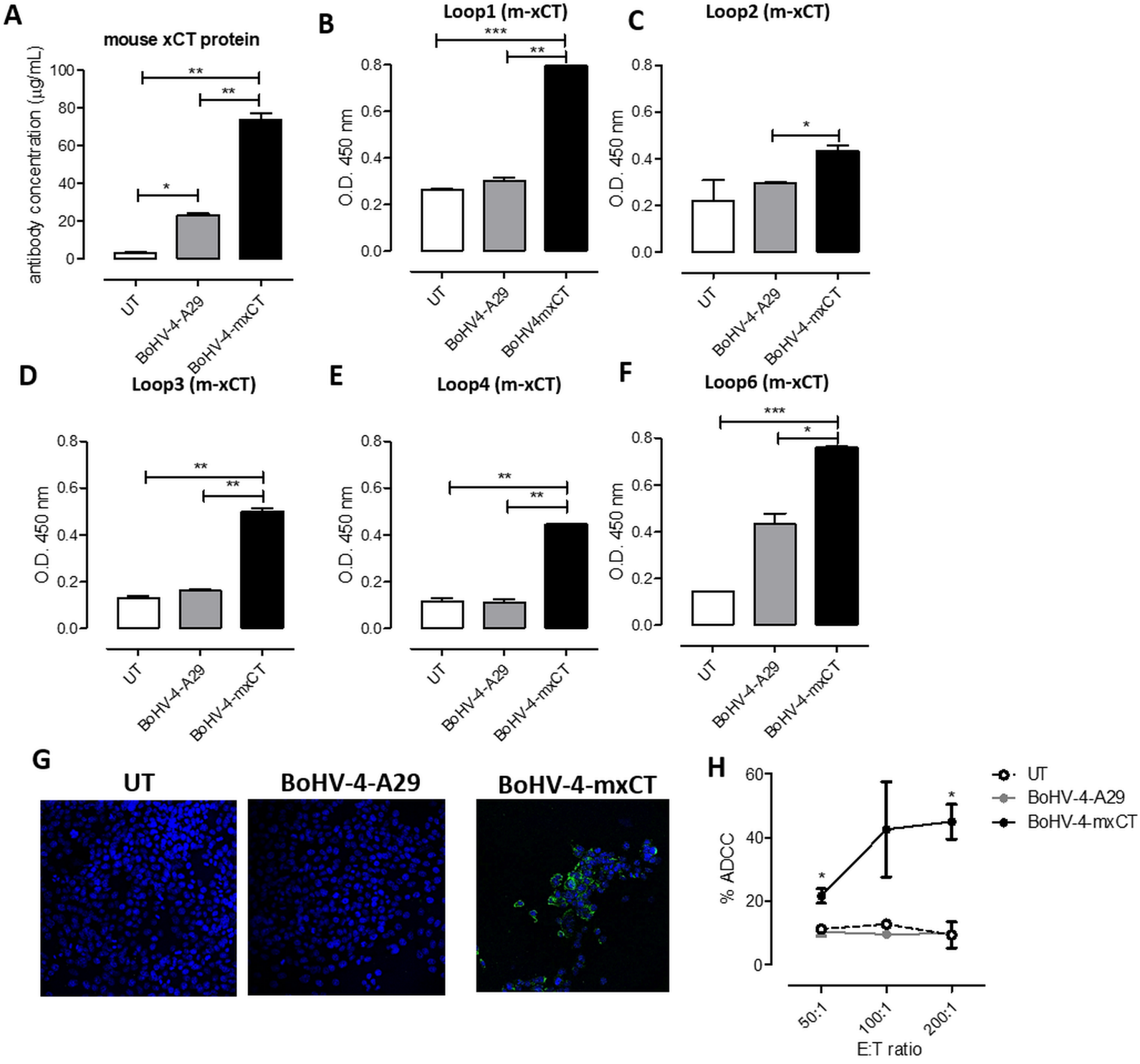
A
mouse xCT protein
antibody concentration (µg/mL)
100
80
60
40
20
0
**
**
*
UT
BoHV-4-A29
BoHV-4-mxCT
B
Loop1 (m-xCT)
***
**
O.D. 450 nm
0.8
0.6
0.4
0.2
0.0
UT
BoHV4-A29
BoHV4mxCT
C
Loop2 (m-xCT)
*
O.D. 450 nm
UT
BoHV-4-A29
BoHV-4-mxCT
D
Loop3 (m-xCT)
**
**
O.D. 450 nm
UT
BoHV-4-A29
BoHV-4-mxCT
E
Loop4 (m-xCT)
**
**
O.D. 450 nm
UT
BoHV-4-A29
BoHV-4-mxCT
F
Loop6 (m-xCT)
***
*
O.D. 450 nm
UT
BoHV-4-A29
BoHV-4-mxCT
G
UT
BoHV-4-A29
BoHV-4-mxCT
H
% ADCC
60
40
20
0
*
*
50:1
100:1
200:1
E:T ratio
UT
BoHV-4-A29
BoHV-4-mxCT

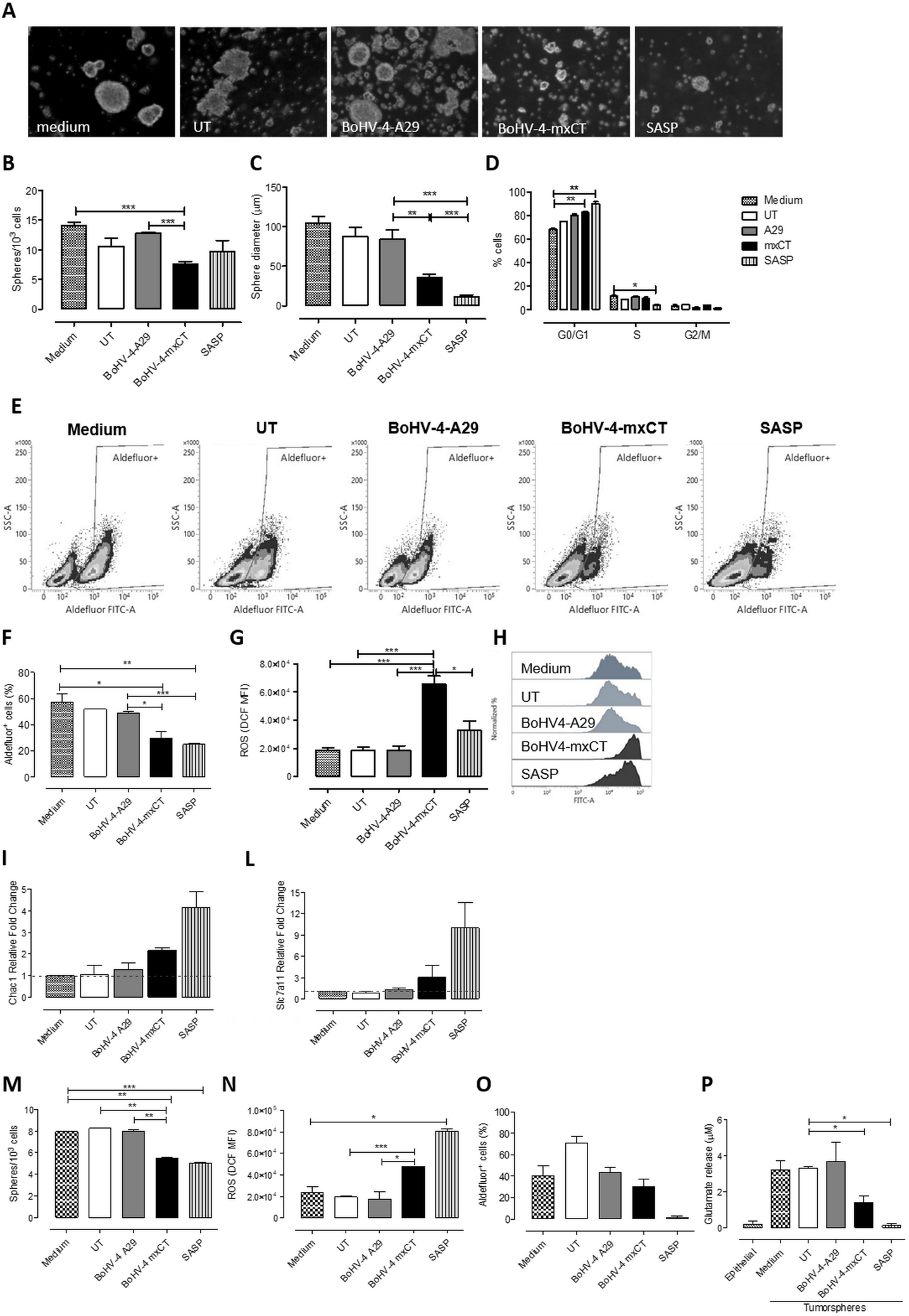
A
medium
UT
BoHV-4-A29
BoHV-4-mxCT
SASP
B
Spheres/10^3 cells
Medium
UT
BoHV-4-A29
BoHV-4-mxCT
SASP
C
Sphere diameter (μm)
D
% cells
G0/G1
S
G2/M
Medium
UT
A29
mxCT
SASP
E
Medium
UT
BoHV-4-A29
BoHV-4-mxCT
SASP
Aldefluor+
SSC-A
Aldefluor FITC-A
F
Aldefluor+ cells (%)
G
ROS (DCF MFI)
H
Medium
UT
BoHV4-A29
BoHV4-mxCT
SASP
Normalized %
FITC-A
I
Chac1 Relative Fold Change
L
Slc 7a11 Relative Fold Change
M
Spheres/10^3 cells
N
ROS (DCF MFI)
O
Aldefluor+ cells (%)
P
Glutamate release (μM)
Epithelial
Medium
UT
BoHV-4-A29
BoHV-4-mxCT
SASP
Tumorspheres

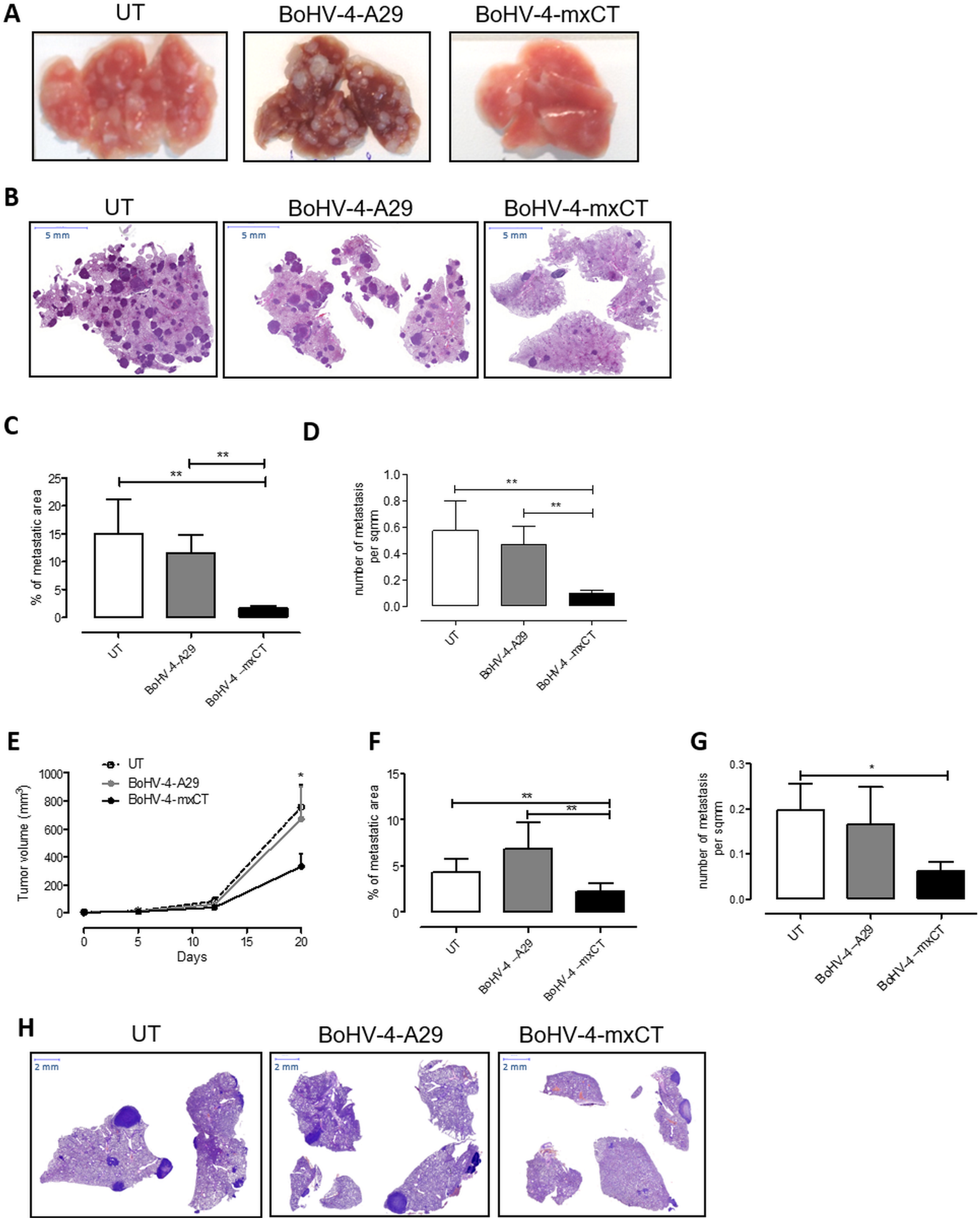
A
UT
BoHV-4-A29
BoHV-4-mxCT
B
UT
BoHV-4-A29
BoHV-4-mxCT
5 mm
C
% of metastatic area
**
**
UT
BoHV-4-A29
BoHV-4 -mxCT
D
number of metastasis per sqmm
**
**
UT
BoHV-4-A29
BoHV-4 -mxCT
E
UT
BoHV-4-A29
BoHV-4-mxCT
Tumor volume (mm3)
Days
*
F
% of metastatic area
**
**
UT
BoHV-4 -A29
BoHV-4 -mxCT
G
number of metastasis per sqmm
*
UT
BoHV-4 -A29
BoHV-4 -mxCT
H
UT
BoHV-4-A29
BoHV-4-mxCT
2 mm

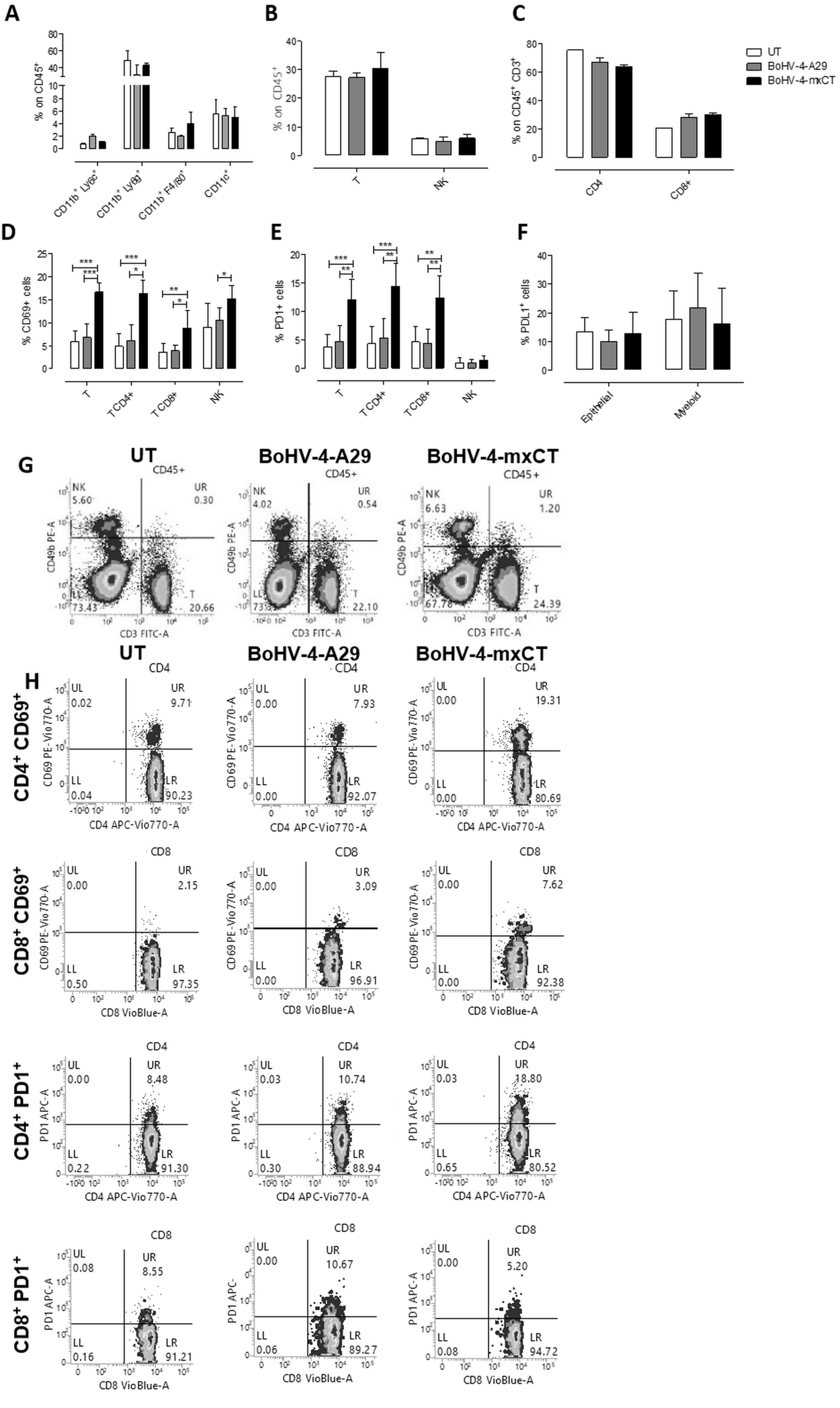
A
% on CD45+
CD11b+ Ly6c+
CD11b+ Ly6g+
CD11b+ F4/80+
CD11c+
B
% on CD45+
T
NK
C
% on CD45+ CD3+
CD4
CD8+
UT
BoHV-4-A29
BoHV-4-mxCT
D
% CD69+ cells
T
T CD4+
T CD8+
NK
E
% PD1+ cells
T
T CD4+
T CD8+
NK
F
% PDL1+ cells
Epithelial
Myeloid
G
UT
BoHV-4-A29
BoHV-4-mxCT
CD45+
NK 5.60
UR 0.30
T 20.66
LL 73.43
NK 4.02
UR 0.54
T 22.10
LL 73
NK 6.63
UR 1.20
T 24.39
LL 67.78
CD49b PE-A
CD3 FITC-A
H
CD4+ CD69+
CD8+ CD69+
CD4+ PD1+
CD8+ PD1+
UT
BoHV-4-A29
BoHV-4-mxCT
CD4
CD8
UL 0.02
UR 9.71
LL 0.04
LR 90.23
UL 0.00
UR 7.93
LL 0.00
LR 92.07
UL 0.00
UR 19.31
LL 0.00
LR 80.69
UL 0.00
UR 2.15
LL 0.50
LR 97.35
UL 0.00
UR 3.09
LL 0.00
LR 96.91
UL 0.00
UR 7.62
LL 0.00
LR 92.38
UL 0.00
UR 8.48
LL 0.22
LR 91.30
UL 0.03
UR 10.74
LL 0.30
LR 88.94
UL 0.03
UR 18.80
LL 0.65
LR 80.52
UL 0.08
UR 8.55
LL 0.16
LR 91.21
UL 0.00
UR 10.67
LL 0.06
LR 89.27
UL 0.00
UR 5.20
LL 0.08
LR 94.72
CD69 PE-Vio770-A
CD4 APC-Vio770-A
CD8 VioBlue-A
PD1 APC-A

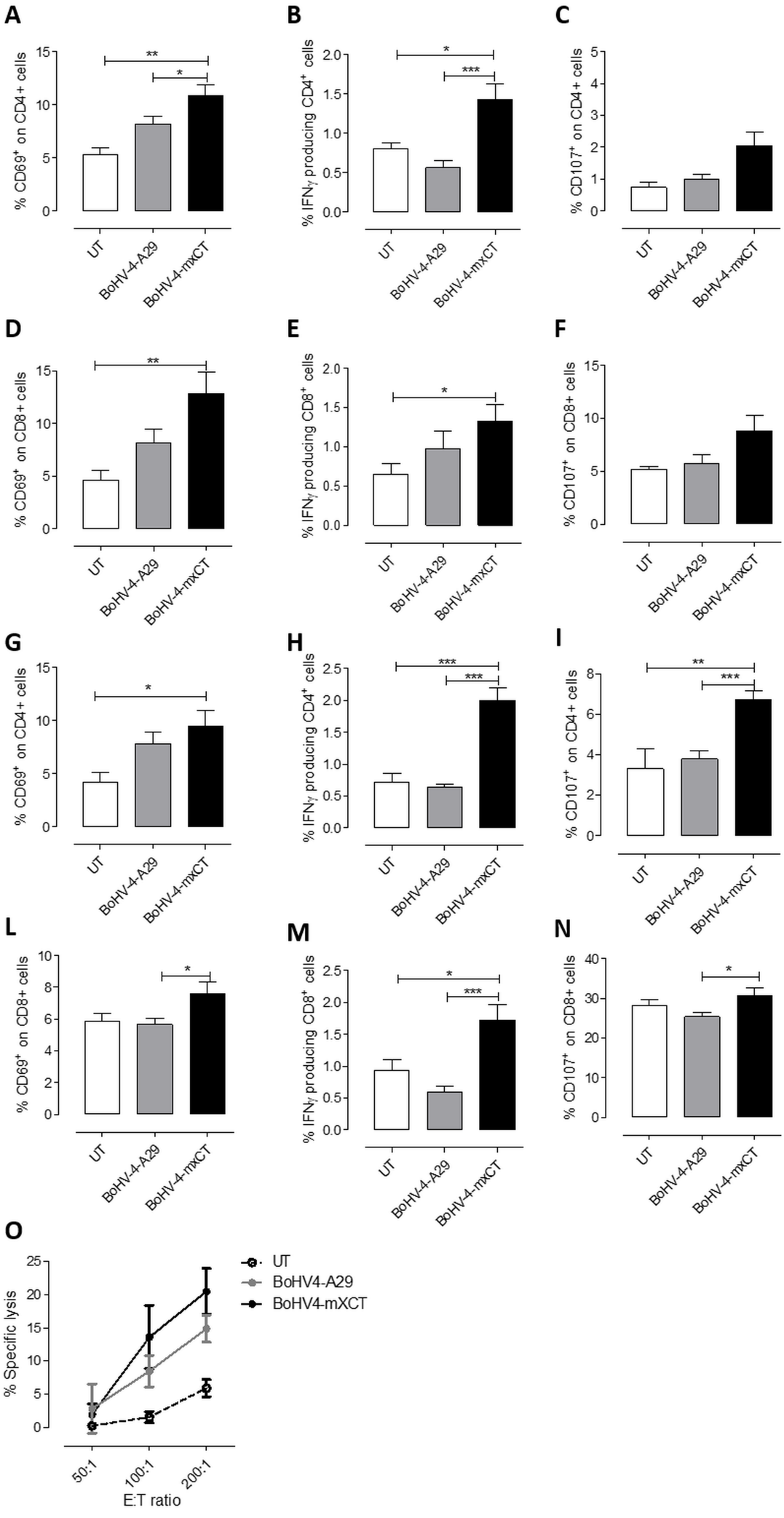
A
% CD69+ on CD4+ cells
B
% IFNγ producing CD4+ cells
C
% CD107+ on CD4+ cells
D
% CD69+ on CD8+ cells
E
% IFNγ producing CD8+ cells
F
% CD107+ on CD8+ cells
G
% CD69+ on CD4+ cells
H
% IFNγ producing CD4+ cells
I
% CD107+ on CD4+ cells
L
% CD69+ on CD8+ cells
M
% IFNγ producing CD8+ cells
N
% CD107+ on CD8+ cells
UT
BoHV-4-A29
BoHV-4-mxCT
O
% Specific lysis
E:T ratio
50:1
100:1
200:1
UT
BoHV4-A29
BoHV4-mXCT

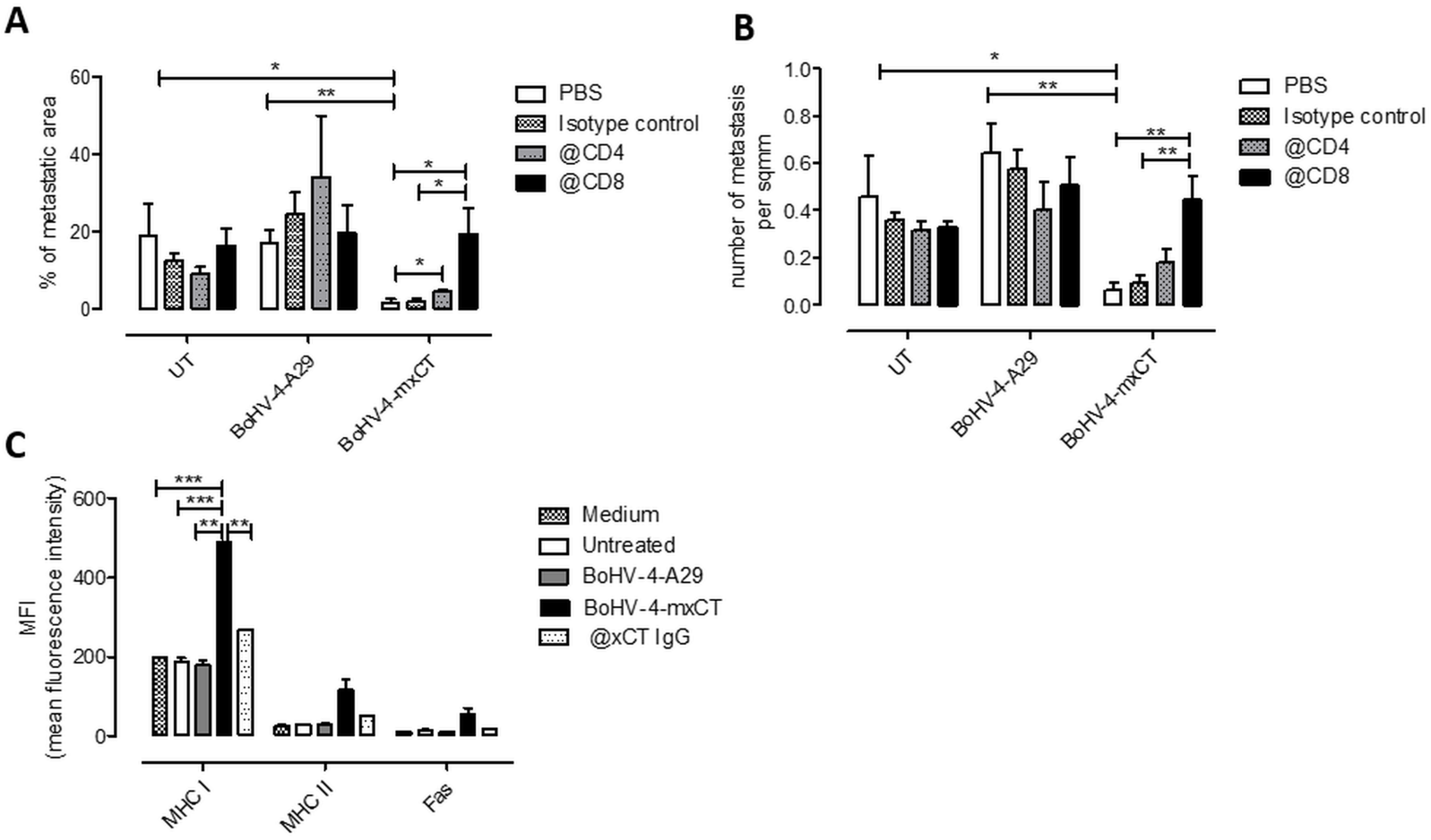
A
% of metastatic area
60
40
20
0
*
**
*
*
*
PBS
Isotype control
@CD4
@CD8
UT
BoHV-4-A29
BoHV-4-mxCT
B
number of metastasis per sqmm
1.0
0.8
0.6
0.4
0.2
0.0
*
**
**
**
PBS
Isotype control
@CD4
@CD8
UT
BoHV-4-A29
BoHV-4-mxCT
C
MFI
(mean fluorescence intensity)
600
400
200
0
***
***
**
**
Medium
Untreated
BoHV-4-A29
BoHV-4-mxCT
@xCT IgG
MHC I
MHC II
Fas

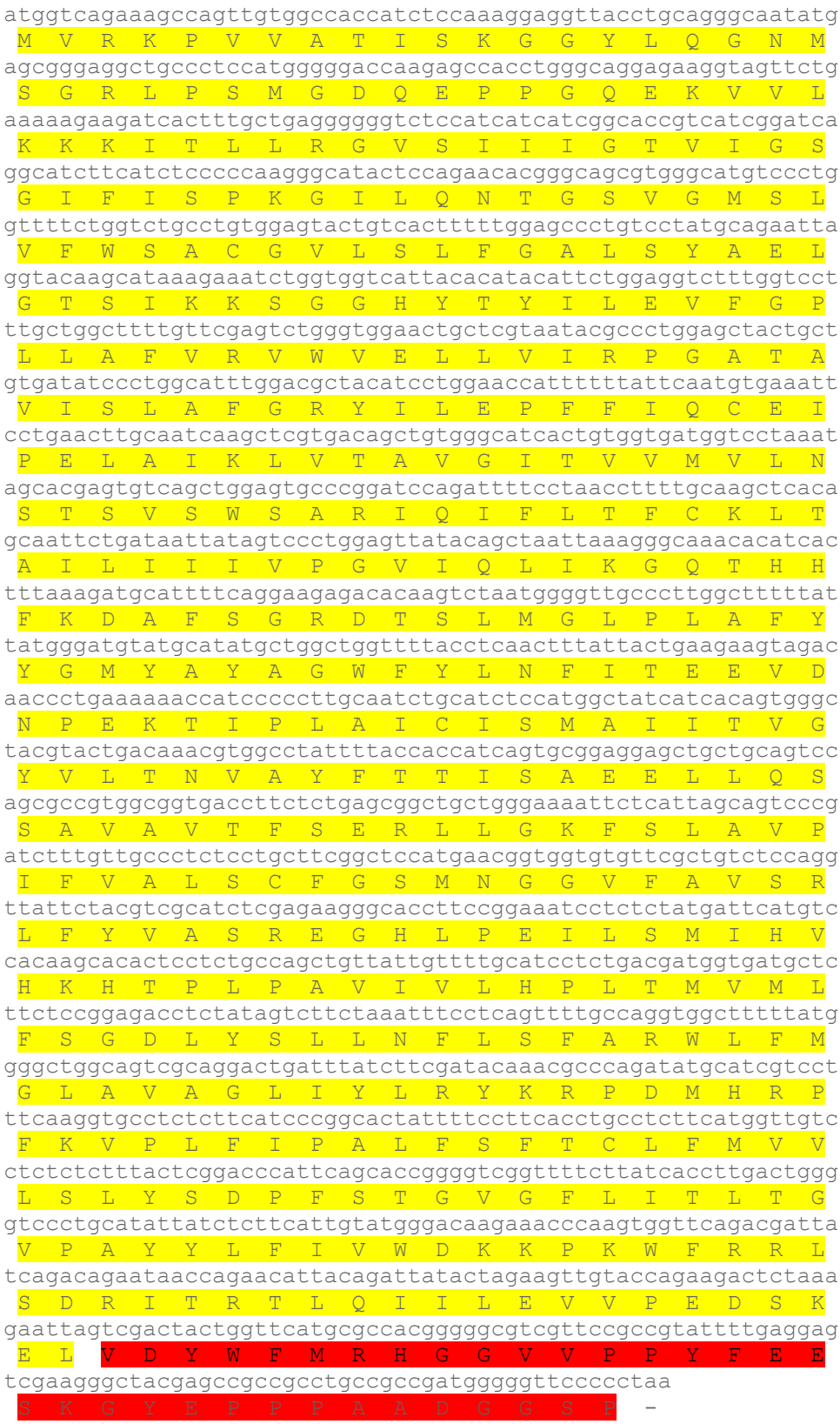

Supplementary Figure 1. A) Mouse xCT (yellow) tagged (red) ORF with deduced amino acids sequence.

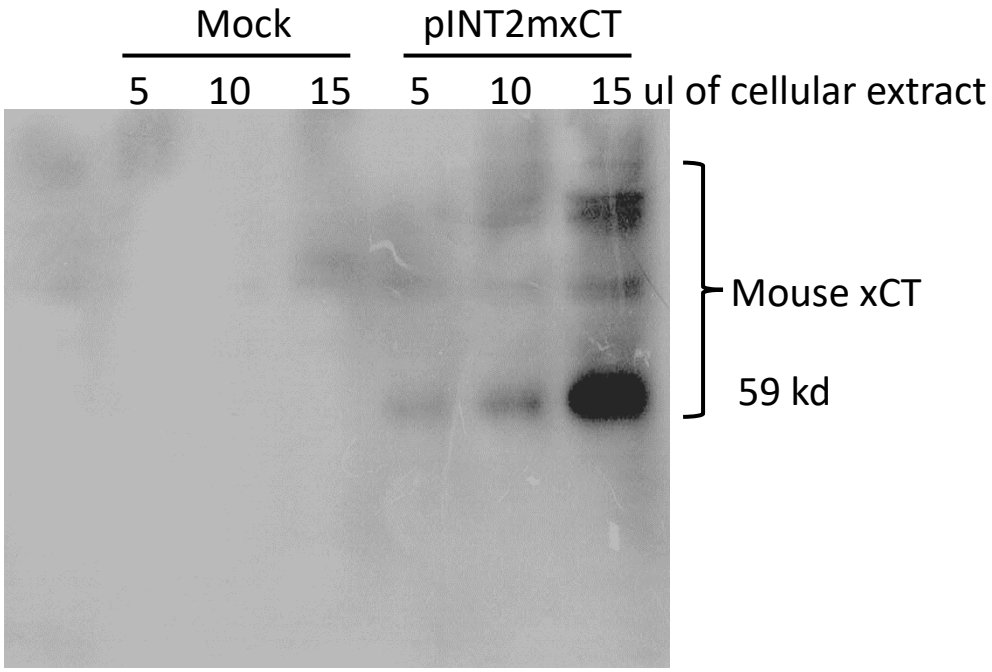

Supplementary Figure S2. pINT2-CMV-mxCTgD$_{106}$ induces xCT expression. pINT2-CMV-mxCTgD$_{106}$ shuttle vector or mock control vector were transiently transfeced into HEK 293T cells. Western immunoblotting of different amounts of total protein cell extracts (5, 10 and 15 μl) using a monoclonal antibody directed against the gD$_{106}$ tag.

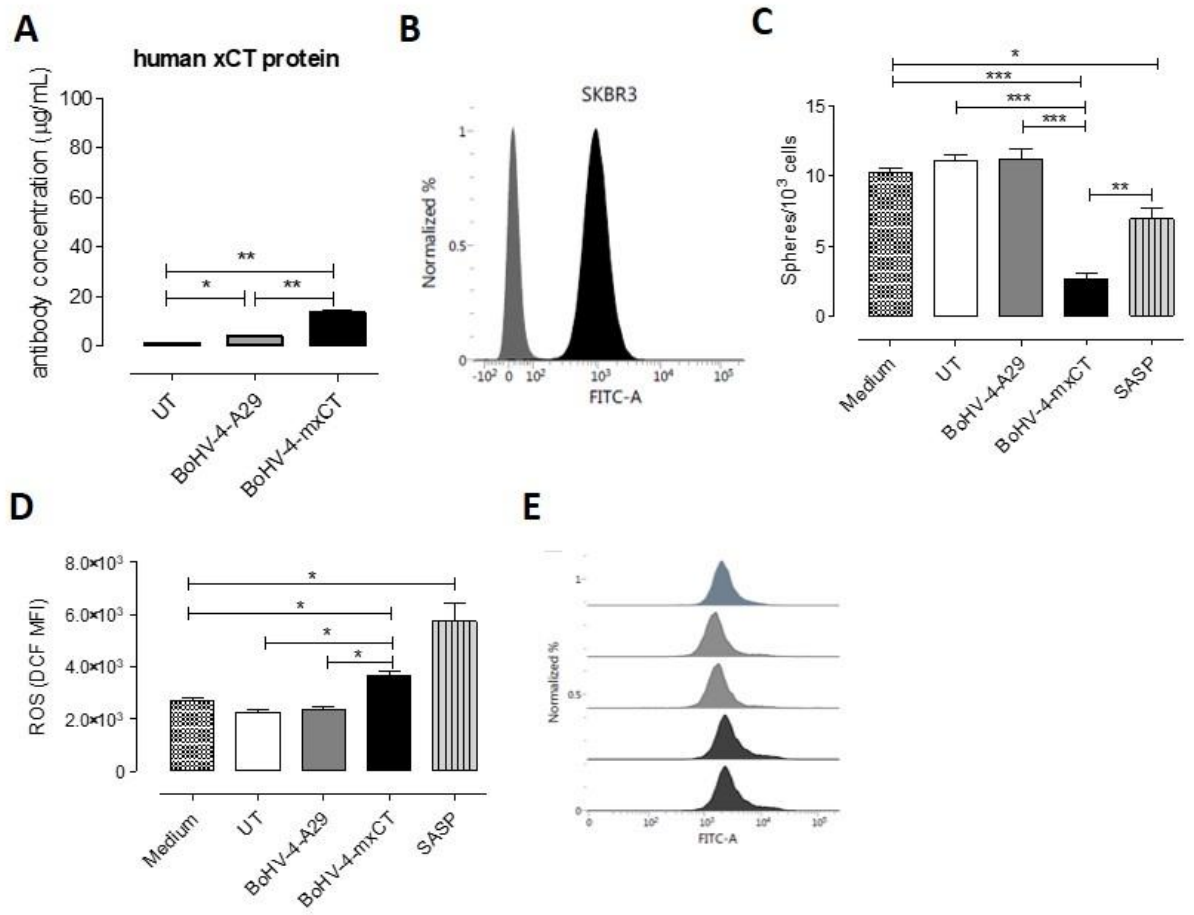

Supplementary Figure S3. BoHV-4-mxCT-induced antibodies affect self-renewal and ROS flux in human CSC. A) Sera from untreated (white bars), BoHV4-A29- (gray bars), and BoHV-4-mxCT- (black bars) vaccinated mice were tested by ELISA on wells coated with full-length human xCT protein. Antibody concentration was calculated based on a standard curve obtained with a commercial anti-xCT antibody targeting its N-terminal region. Graph shows mean ± SEM of sera pooled from 3 independent experiments. **B)** FACS analysis of xCT expression on tumorspheres generated from $Her2^+$ human SKBR3 cells stained with control Ig (gray histogram) or rabbit anti-xCT (black histrogram). **C-E)** SKBR3-derived tumorspheres were incubated for 5 days with medium, sera of BALB/c mice left untreated or vaccinated with BoHV-4-A29 or BoHV-4-mxCT, or with SASP (50 µM). **C)** Sphere generating ability reported as tumorsphere number/10^3 plated cells. **D, E)** FACS analysis of ROS production, reported as DCF MFI or shown as representative histograms.